the scattered intensity $I(q)$ can be written as the product of the form factor $P(q)$ of the bilayers and the structure factor $S(q)$ describing their spatial arrangement similarly to that of globular particle systems

$$I(q) \propto P(q)S(q) \tag{6}$$

When the thickness of the bilayer is sufficiently smaller than the length scale of the remaining two other dimensions as well as the radius of curvature of the bilayer, the form factor $P(q)$ in eq 6 can be replaced with the product of the so-called Lorentz factor, $1/q^2$, and the thickness form factor or scattering function, $P_t(q)$,[58]

$$P(q) = (2\pi A/q^2)P_t(q) \tag{7}$$

where A is the area of the basal plane. Substituting $P_t(q)$ for $P(q)$, $I(q)$ in eq 6 can be rewritten in the convenient form

$$I(q) \propto P_t(q)S(q)/q^2 \tag{8}$$

The thickness scattering function $P_t(q)$ is the cosine transformation of the thickness distance distribution function (thickness PDDF) $p_t(r)$. Therefore, we can use a similar method to a conventional indirect Fourier transformation (IFT)[59] to deduce $p_t(r)$ from the experimental $P_t(q)$[58]

$$P_t(q) = 2\int_0^\infty p_t(r)\cos(qr)\mathrm{d}r \tag{9}$$

In the case of the absence of interlamellar interference peaks and their signature (no bilayer stacking as to be expected for vesicle solutions), we can assume $S(q) = 1$ in eq 6. Figure 2c presents the calculated thickness PDDF, $p_t(r)$, of the vesicle designed for Hb encapsulation. We have already shown that the surface modification with low density poly(ethyleneglycol) (PEG) is quite efficient for long-term storage of the HbV, inhibiting intervesicular aggregation and fusion.[48,60] However, due to the low density of PEG for surface modification of the vesicle as the concentration of DSPE-PEG is as low as 0.3 mol % of the total lipids, we were not able to observe the effect of PEG in $p_t(r)$. Nevertheless, $p_t(r)$ deduced without using any geometrical model reveals the thickness of the bilayer excluding PEG layer to be ca. 5.8 nm, which is read out from the distance (r-value) where $p_t(r)$ goes to zero, as highlighted in Figure 2c. Recently, we studied static structure and molecular dynamics in PEG-lipid (DSPE-PEG) micellar solutions with different molecular weights of PEG, M_{PEG}, by means of SAXS and dielectric relaxation spectroscopy (DRS).[61] The thickness of the hydrated PEG layer was estimated to be 8−9 nm for M_{PEG} = 5000. Because of different density and configuration, the extension of polymer chains in solution may not necessarily be identical in the micelle and on the surface of the vesicle, and it is apparent that the actual total bilayer thickness involving the surface PEG layer must be far greater than 5.8 nm.

The positive−negative−positive behavior of $p_t(r)$ when going from $r = 0$ to higher r values is directly connected to the occurrence of positive and negative internal electron density layers within the bilayer. Theoretically, $p_t(r)$ is given by the convolution square of the electron density profile $\Delta\rho_t(r)$ perpendicular to the midplane of the bilayers, which is given by

$$p_t(r) = 2\int_0^\infty \Delta\rho(r')\Delta\rho(r' + r)\mathrm{d}r' \tag{10}$$

To extract more intuitive pictures of the internal structure of the bilayer, we performed a deconvolution procedure of the experimental $p_t(r)$ into $\Delta\rho_t(r)$ using a convolution square-root technique.[62−64] In Figure 2d, we display $\Delta\rho_t(r)$ obtained from the deconvolution analysis of $p_t(r)$ shown in Figure 2c. The innermost (the smallest-r) negative density part apparently reflects hydrophobic chain of the lipids. The following plateau having nearly zero electron density fluctuation or an identical electron density with that of solvent water including salt, indicates localized cholesterol molecules on the hydrophobic/hydrophilic interface.[65] A terminal hydroxyl group is expected to be oriented toward the hydrophilic site of the lipids. The positive density layer seen in $1.7 \leq r/\mathrm{nm} \leq 2.9$ is attributed to the hydrophilic headgroup of the lipids. We note that the forward SAXS intensity is generally very sensitive not only to the structure but also the temperature dependent contrast. The pronounced difference in the forward intensities and different positions of the minimum in $I(q)$ at different temperatures as shown in Figure 2b sensitively reflect different contrast as a function of temperature. IFT and deconvolution analyses[62−64] given in Figure 2c, d demonstrate the stable bilayer structure, which does not significantly depend on temperature.

Hierarchical Structures of HbV and the Solution State of the Encapsulated Hbs. The HbVs are hierarchically organized cellular-type artificial oxygen carrier that encapsulates a concentrated Hb solution in phospholipid vesicles, one HbV particle containing ca. 30 000 Hb molecules. Figure 3 shows the SAXS intensity, $I(q)$, of the concentrated HbV dispersion ([Hb] = 10 g dL^{-1}, [solutes] = 16 g dL^{-1}; volume fraction, ca. 40%). We successfully measured more than 5 orders of magnitude of the scattered intensity (ca. 3.5×10^5 time different maximum and minimum intensities), covering the extremely wide q-range of 0.06−10 nm^{-1}, which was quite essential for exploring the internal structures of HbV at the molecular level.

First, we checked the concentration dependence of $I(q)$ by diluting the dense stock HbV dispersion ([Hb] = 10 g dL^{-1}) with saline solution, and found virtually no concentration dependence of the shape of the scattering functions. This means that the effect of interparticle interactions or static structure factor $S(q)$, which is given as the Fourier transform of the total correlation function [$g(r)$-1] and whose first peak position is expected to be $q = \sim 0.025$ nm^{-1} when hardsphere (HS) interaction and a 120 nm radius are assumed, is not visible on the experimental $I(q)$ in our accessible q-range ($q > 0.06$ nm^{-1}). Consistent with the DLS results, the forward intensity of the HbV dispersion exhibits a typical feature of to some extent polydisperse spherical particles. In Figure 3, we added a theoretical scattering function calculated by accounting for the averaged diameter (~240 nm) and the size distribution obtained by DLS (green line, adjusted in height to the experimental intensity). Suppose that the HbV has homogeneous electron density distribution inside the particle, $I(q)$ should rapidly decrease proportional to q^{-4}, according to the theoretical curve for homogeneous spheres. However, we clearly observed an enhanced excess scattering in the regime $2 \leq q/\mathrm{nm}^{-1} \leq 10$. This high-$q$ excess component manifests the internal electron density fluctuations of the HbV particle, reflecting the shorter length scale structures of the encapsulated Hb solution and the lipid bilayer.

If we carefully look at the two specific q-ranges indicated by the two squares placed in Figure 3a, which are magnified in

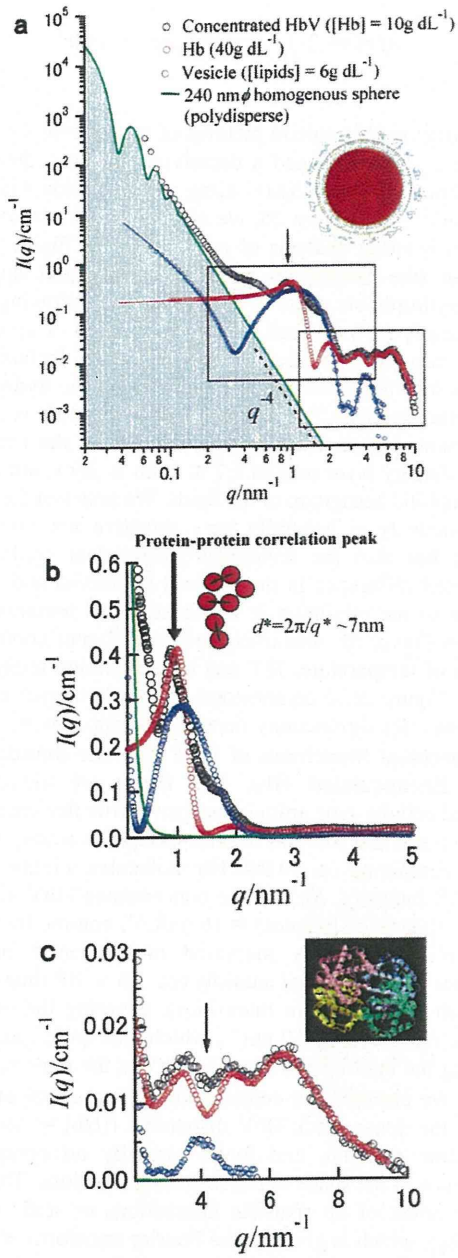

Figure 3. X-ray scattered intensity $I(q)$ in a log−log plot of the concentrated HbV dispersion ([Hb] = 10 g dL^{-1}) at 25 °C in 0.06 ≤ q/nm^{-1} ≤ 10 is shown on absolute scale. A schematic picture of HbV is inserted into the panel a as well as a simulated scattering curve of a solution of polydisperse spheres according to the DLS results. In the panels b and c, the enlarged views of the high-q range are displayed in a lin−lin plot to visualize the significant features of $I(q)$ for protein−protein correlation peak and microscopic intramolecular structure of the encapsulated Hbs. Molecular structure of Hb is inserted in the panel c.

Figure 3b, c, we are able to access the information on the protein−protein interactions in the confined space of the aqueous phase of the HbV and the microscopic intra molecular structure of Hb molecules. As shown in Figure 3b, c, we found that the high-q part of $I(q)$ of the HbV is well approximated by a superposition of the experimental scattering functions of the concentrated Hb solution with identical concentration (ca. 38 g dL^{-1}) and of the phospholipids bilayer membrane (empty vesicles). Generally, for globular colloidal particle systems like proteins and micelles, the position, height, and width of the first

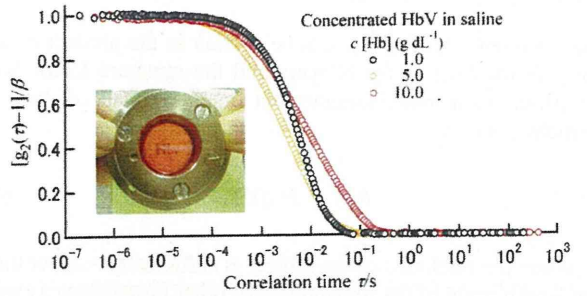

Figure 4. The normalized intensity correlation functions, $[g_2(\tau) - 1]/\beta$, of the concentrated dispersions of the HbV at [Hb] = 1.0, 5.0, and 10 g dL^{-1}, as obtained by a modified TC-DLS technique at q = 6.75 × 10^{-3} nm^{-1}.

peak of $S(q)$ strongly depends on the interparticle interactions determined, for example, by the radius, volume fraction, effective charge of the particles, a screening effect of electrostatic interaction, surface adhesion, and so forth.[53,61,66−69] The details of the concentration and temperature dependence of the Hb−Hb interactions in relation to the biological functions of Hb will be reported elsewhere. Importantly, we found that the protein−protein correlation peak position as well as the height and width of the first peak of $S(q)$ of the encapsulated Hbs are almost identical to those of a normal Hb solution with identical concentration (Figures 3b). The finding suggests that confinement effects into a ca. 240 nm ϕ space are not very significant for the interparticle interaction potential of Hbs.

Figure 3c confirms the perfect coincidence of the scattering functions for the encapsulated and normal (bulk) Hbs in 2 ≤ q/nm^{-1} ≤ 10, where the small difference between those of HbV and the normal Hb solution seen in 3 ≤ q/nm^{-1} ≤ 5, highlighted by an arrow, can clearly be explained in terms of the contribution from the encapsulating vesicle. This implies unbiased intramolecular structures of Hb before and after its encapsulation into HbV.

Particle Diffusion Dynamics in a Concentrated HbV Dispersion. One of the most significant specificities of the HbV compared to any other conventional liposomal products is its extremely high concentration ([Hb] = 10 g dL^{-1}; [lipids] = 6 g dL^{-1}). This comes essentially from the requirement for achieving an oxygen-carrying capacity comparable to that of blood. As a result, the HbV dispersion for practical medical use is totally turbid due to high concentration and the submicrometer particle size. DLS techniques are often successfully used for observing diffusion processes of particle systems, thus being efficient for characterizing microscopic motion and interparticle interactions of particles. However, conventional DLS techniques that rely on a singly scattered signal are no longer applicable for such a dense, turbid system because of multiple scattering. In addition, absorption of hemoprotein is also a specific problem for the HbV system to overcome. Therefore, we needed to efficiently reduce the scattering volume of the sample to observe microscopic motions of the HbV particles without diluting the samples. To overcome the obstacles, we used a modified thin-layer cell dynamic light-scattering (TC-DLS) technique.[42,43] As shown in the inset of Figure 4a, the concentrated HbV ([Hb] = 10 g dL^{-1}) dispersion inserted into the thin-layer cell (50 μm thick) is transparent as if it were a red cellophane sheet. The opposite side can be seen through the TC window, as "HbV" written on a paper is readable without mistiness, and thus DLS experiments in the forward direction become possible. The total scattering angle in air was fixed to 41° for all the experiments, which corresponds to 29° in water, resulting in q = 6.75 × 10^{-3} nm^{-1}.

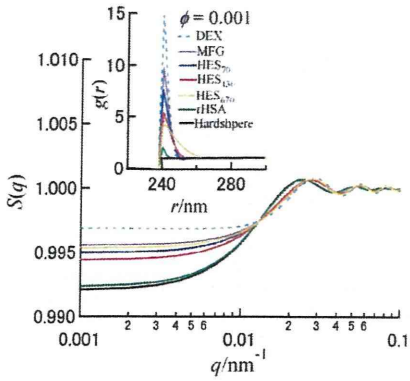

Figure 5. Simulated static structure factors $S(q)$ and pair correlation functions $g(r)$ of the model systems accounting for a dilute HbV suspended in the series of plasma substitutes. $g(r)$ and $S(q)$ were calculated using a depletion interaction potential for monodisperse hardspheres in the presence of nonadsorbing polymers and SMSA closure relation. We chose the diameter $\sigma = 240$ nm and volume fraction $\phi = 0.001$ to account for HbV in a dilute suspension, and the diameter $2R_g$ for small particles (polymers), where radius of gyration of the plasma substitutes determined by SAXS at $c = 1.0$ g dL^{-1} (unpublished results) was used for R_g. We assumed the situation that HbVs are suspended in plasma substitutes having half of the original concentration, that is, 2.5 g dL^{-1} (rHSA), 5.0 g dL^{-1} (DEX), 2.0 g dL^{-1} (MFG), 3.0 g dL^{-1} (HES_{70}), 3.0 g dL^{-1} (HES_{130}), and 3.0 g dL^{-1} (HES_{670}).

Figure 4 shows the concentration dependence of the normalized intensity correlation functions, $[g_2(\tau) - 1]/\beta$, of the concentrated HbV dispersions measured at $q = 6.75 \times 10^{-3}$ nm^{-1}, which is lower than an anticipated HbV−HbV correlation peak position $q \sim 0.025$ nm^{-1} (See Figure 5). With increasing concentration from [Hb] = 1 g dL^{-1} to 5 g dL^{-1}, the short-time decay of $g_2(\tau)$ becomes faster, as excepted for the corrective diffusion of all repulsively interacting HS systems. At the same time, we found the stretch of the long-time tail of $g_2(\tau)$, which may seem to indicate the occurrence of the gradual slowdown of the long-time behavior. With the further increase to [Hb] = 10 g dL^{-1}, in turn, the short-time decay of $g_2(\tau)$ becomes slower, which is opposite to what is anticipated for a repulsively interacting system, and may imply the existence of weak attractive (adhesive) potential between HbVs. We may need to perform further experimental works to seek to understand the details of the interaction potentials between the HbVs. Nevertheless, the present TC-DLS data confirm that $g_2(\tau)$ for the most concentrated stock HbV dispersion ([Hb] = 10 g dL^{-1}) rapidly converges to the baseline (unity) showing single-step behavior, which demonstrates from a viewpoint of the particle diffusion dynamics that the HbV dispersion is an ergodic system. The finding well supports good dispersion stability and proved long-term preservation, owing to the applied surface modification of the HbV with poly(ethylene glycol) (PEG).

The Effect of Plasma Substitutes on HbV−HbV Interactions. Since the HbV does not contribute to COP of blood, upon anticipated actual medical treatments the HbV must be dispersed with aqueous solution of plasma substitutes (water-soluble polymers) to adjust COP. Recently, Sakai et al. reported the rheological properties of the HbV dispersion ([Hb] = 10 g dL^{-1}) in a series of plasma substitute solutions with various molecular structures and molecular weights, such as rHSA, DEX, MFG, and HES.[32] They found that among these polymers, only HbV suspended in rHSA behaves nearly as a Newtonian fluid. In contrast, other plasma substitutes, such as HES, DEX, and MFG, induce non-Newtonian behavior of the HbV dispersions in particular for high molecular weight HES. Microchannel flow experiments indicated that this is due to flocculation of HbV in the presence of plasma substitutes. To gain insights into the mechanism of the HbV flocculation, we use different DLS techniques in this section.

Simulated Static Structure Factors with Depletion Interaction Potential. The depletion interaction potential[26−28] for hardsphere having the diameter σ in the presence of nonadsorbing polymers with the radius of gyration R_g can be approximated in the range of $\sigma < r < \sigma + 2R_g$ as[29]

$$u(r) = -\eta_p^{(R)} k_B T \frac{3}{2} \frac{1+\xi}{\xi^3} \left(\frac{r}{\sigma} - 1 - \xi \right)^2 \qquad (11)$$

where r is the center-of-mass to center-of-mass distance between the two particles, $\xi = 2R_g/\sigma$ is the size ratio, corresponding to the dimensionless range of the depletion attraction, $\eta_p^{(R)}$ is the reservoir polymer volume fraction, which can be calculated from the volume fraction of the large particles ϕ and the size ratio ξ.[30] From eq 11, one can easily find that the depth of the depletion potential is closely related to the two key parameters of ξ and $\eta_p^{(R)}$; the stronger attractive force between the two large particles is induced for smaller ξ and larger $\eta_p^{(R)}$. We simulated the pair correlation functions, $g(r)$, and the resulting static structure factors, $S(q)$, for the model systems of a very diluted HbV suspended in a series of plasma substitutes using depletion interaction potential model and SMSA closure relation.[70,71]

In Figure 5, we present $g(r)$ and $S(q)$ calculated assuming the diameter $\sigma = 240$ nm and volume fraction $\phi = 0.001$ to account for the HbV. To give ξ, the radius of gyration of the plasma substitutes determined by SAXS at $c = 1.0$ g dL^{-1} (unpublished results) was used: 5.5 nm (MFG), 4.96 nm (DEX), 2.84 nm (rHSA), 5.96 nm (HES_{70}), 6.83 nm (HES_{130}), and 12.95 nm (HES_{670}). The solution structures of these plasma substitutes, involving the Flory radius, screening length, persistence length, and length scale-dependent fractal dimensions of the polymer chains will be reported elsewhere. We selected half of the original concentration of commercially available plasma substitutes; 2.5 g dL^{-1} (rHSA), 5.0 g dL^{-1} (DEX), 2.0 g dL^{-1} (MFG), 3.0 g dL^{-1} (HES_{70}), 3.0 g dL^{-1} (HES_{130}), and 3.0 g dL^{-1} (HES_{670}). In these calculations, we rely on the depletion potential and SMSA closure. According to the theoretical phase diagram,[30,31] the selected concentration of DEX seems to be already in the two phase region even at such a dilute concentration of the vesicle (to distinguish, $S(q)$ and $g(r)$ for DEX are given using a dashed line), while theoretically, others are still in one-phase fluid region.

In terms of the increased osmotic compressibility and coordination number manifested respectively in the $S(q)$ and $g(r)$, we estimated the effect of the different plasma substitutes on the flocculation tendency of the HbV particles to be in the order of DEX > MFG> HES_{670} > HES_{70} > HES_{130} > rHSA. We will examine the validity of this prediction using DLS technique in the next subsection.

Effects of Plasma Substitutes on the HbV Diffusion Dynamics in a Diluted Dispersion. To start with the simplest case, we first tried to investigate variation of the particle diffusion dynamics of the vesicle (without Hb encapsulation) in a diluted suspension in the presence of plasma substitutes and its polymer-concentration dependence. Figure 6 shows the intensity correlation functions, $g_2(t)$, of a diluted vesicle ([lipids] = 0.012 g dL^{-1}) dispersed in various plasma substitute solutions of rHSA, DEX, MFG, HES_{70}, HES_{130}, and HES_{670}, measured at $q = 0.223$ nm^{-1}. The concentrations of these plasma

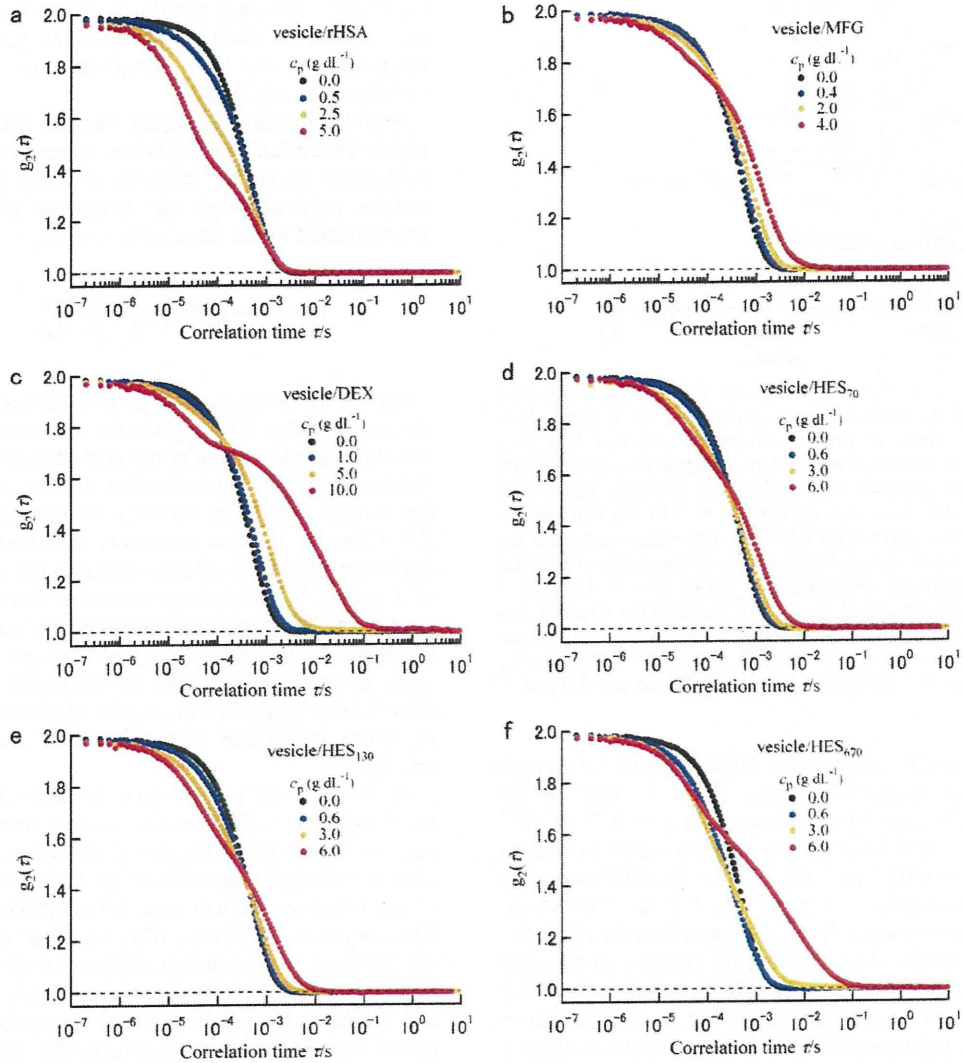

Figure 6. The intensity correlation functions, $g_2(t)$, of a 0.012 g dL^{-1} vesicle suspended in various plasma substitute solutions of rHSA, DEX, MFG, HES_{70}, HES_{130}, and HES_{670}, measured at $q = 0.223$ nm^{-1}. The concentrations of the plasma substitutes are adjusted to 10, 50, and 100% of their original concentration by dilution with saline solution.

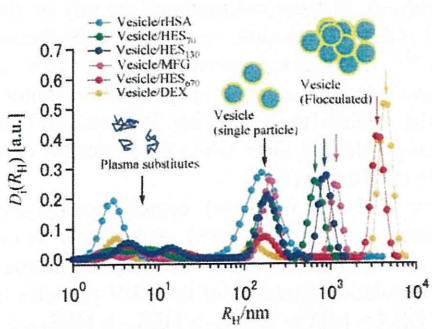

Figure 7. Effect of plasma substitutes on vesicle flocculation in a dilute suspension. The intensity distribution functions, $D_i(R_H)$, of a 0.012 g dL^{-1} vesicle suspended in various plasma substitute solutions of rHSA, DEX, MFG, HES_{70}, HES_{130}, and HES_{670} as a function of hydrodynamic radius, R_H. $D_i(R_H)$ was calculated form the intensity correlation functions, $g_2(t)$, presented in Figure 6 using ORT procedure.[56]

substitutes are varied from 10 to 100% of their original concentrations, while fixing vesicle concentration. Figure 7a shows $g_2(t)$ of the vesicle/rHSA systems. With increasing rHSA concentration, two distinct decays become clearly visible. The faster decay is apparently attributed to the diffusion of rHSAs, and the slower one is to that of the vesicles. Importantly, we observed that $g_2(t)$ at different rHSA concentrations almost simultaneously converges to the baseline at about the same point, demonstrating that a significant slowdown of the vesicle diffusion is not induced by rHSA.

The appearance of two distinct decays is common for all polymers. However, in contrast to the case of rHSA, we found that, as can be seen from Figure 6b–e, all other plasma substitutes cause a pronounced slowdown of the vesicle translational diffusion, and the effect becomes significantly stronger with increasing polymer concentration. In Figure 7, we display the intensity distribution functions $D_i(R_H)$ of vesicle dispersions calculated using ORT[56] from the same DLS data shown in Figure 6a–f, where the data at highest plasma substitute concentrations were chosen. Figure 7 underlines that rHSA does not cause the vesicle flocculation, but other polymers do. In terms of $D_i(R_H)$, the efficacy of the plasma substitutes on the vesicle flocculation are estimated to be in the order of DEX > HES_{670} > MFG > HES_{130} > HES_{70} > rHSA, instead of DEX > MFG> HES_{670} > HES_{70} > HES_{130} > rHSA that is predicted from the depletion potential model. In light of the results, the tendency can broadly be explained with depletion interaction, but there exists some singularity of HES series: (i) the influence of HES_{670} is considerably stronger than expected

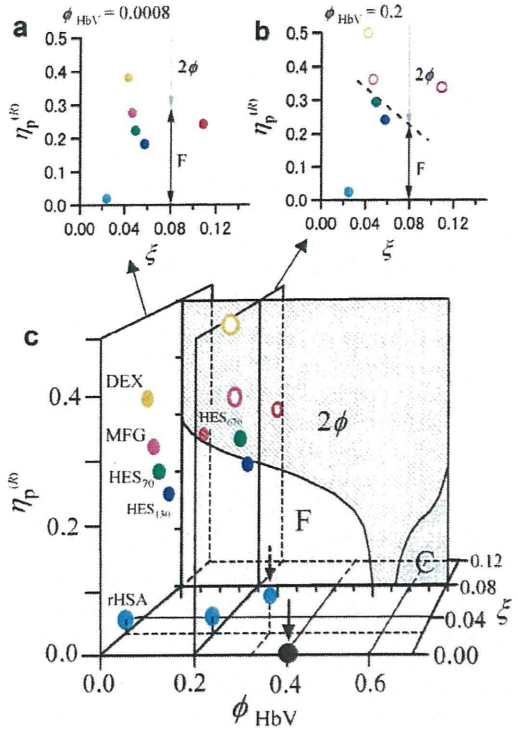

Figure 8. Partial phase diagram of HbV in the presence of plasma substitutes as a function of HbV volume fraction ϕ_{HbV}, reservoir polymer volume fractions $\eta_p^{(R)}$, and the polymer to HbV size ratio ξ, shown together with a theoretical phase diagram of a colloid−polymer mixture ($\xi = 0.08$).[27] Panels a and b represent 2D phase diagrams at ϕ_{HbV} = 0.0008 and ϕ_{HbV} = 0.2, respectively, and c presents a 3D diagram as a function of ϕ_{HbV}, $\eta_p^{(R)}$, and ξ. F, C, and 2ϕ on the theoretical phase diagram indicate single phase fluid, crystal, and two phase regions, respectively. For ϕ_{HbV} = 0.0008 and 0.2, the concentration of plasma substitutes was fixed to half of their original ones, that is, 2.5 g dL^{-1} (rHSA, light blue), 5.0 g dL^{-1} (DEX, orange), 2.0 g dL^{-1} (MFG, pink), 3.0 g dL^{-1} (HES_{70}, bright green), 3.0 g dL^{-1} (HES_{130}, blue), and 3.0 g dL^{-1} (HES_{670}, red). Filled and empty circles represent single phase fluid and two-phase, respectively. Arrows highlight the stock HbV dispersion (ϕ_{HbV} = 0.4) and a currently major applicatory HbV/rHSA mixture (ϕ_{HbV} = 0.32) used for preclinical tests.

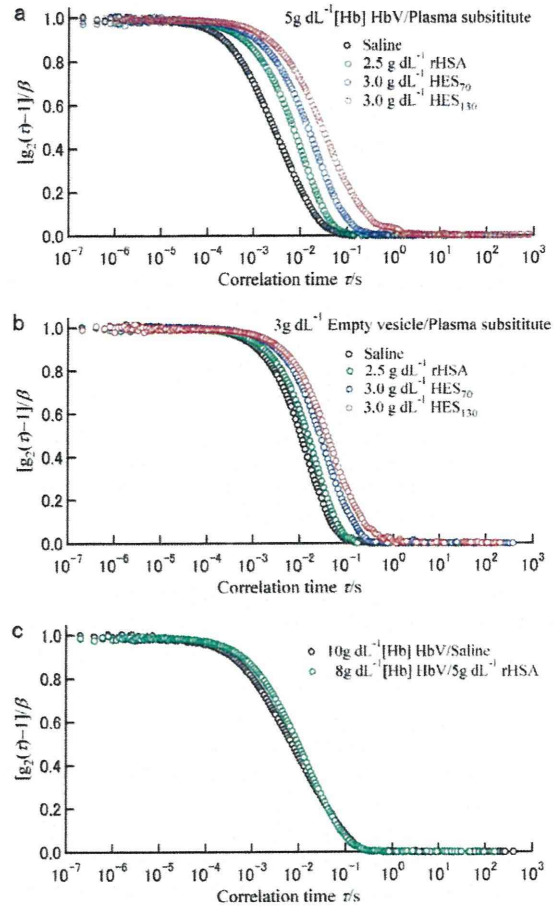

Figure 9. The normalized intensity correlation functions, $[g_2(\tau)-1]/\beta$, of the concentrated dispersions of HbV and empty unilamellar vesicles in saline and plasma substitute solutions; the HbV ([Hb] = 5.0 g dL^{-1}) suspended in 2.5 g dL^{-1} rHSA, 3.0 g dL^{-1} HES_{70}, and 3.0 g dL^{-1} HES_{130} solutions. (a) the 3.0 g dL^{-1} vesicle in the same series of plasma substitutes (b), and the stock HbV dispersion ([Hb] = 10 g dL^{-1}) and the applicatory HbV ([Hb] = 8 g dL^{-1}) in a 5 g dL^{-1} rHSA dispersion in actual medical applications (c).

and (ii) the effect of HES_{130} is stronger than that for HES_{70}, which is opposite to the theoretical prediction. These are likely to be due to unideality of the systems involving the distribution of molecular weights and the complexity of the polymer chain structure.

In Figure 8, a partial phase diagram of HbV/polymer mixtures as a function of ϕ_{HbV}, $\eta_p^{(R)}$, and ξ is presented together with a typical theoretical phase diagram of a colloid−polymer mixture ($\xi = 0.08$),[27] where the reservoir polymer volume fractions $\eta_p^{(R)}$ are estimated for different plasma substitutes at half of their original concentrations; 2.5 g dL^{-1} (rHSA), 5.0 g dL^{-1} (DEX), 2.0 g dL^{-1} (MFG), 3.0 g dL^{-1} (HES_{70}), 3.0 g dL^{-1} (HES_{130}), and 3.0 g dL^{-1} (HES_{670}), using the radius of gyration R_g determined with SAXS data at 1.0 g dL^{-1} (unpublished data). The filled and empty circles represent single liquid and two phases, respectively. In practice, other conditions, for example, polydispersity and surface charge of the large particle as well as nonideality of polymer structure especially at high $\eta_p^{(R)}$ may affect the phase behavior. Nevertheless, the figure implies that the phase separation of the HbV suspension in the presence of the plasma substitutes can be understood based on the depletion interaction potential model for hardsphere mixed with nonadsorbing polymers.

The Effects of Plasma Substitutes on the HbV Diffusion Dynamics in a Dense Dispersion. We used TC-DLS to study concentrated HbV/plasma substitute mixtures. In Figure 9a, b, we present $g_2(t)$ of the concentrated HbV ([Hb] = 5 g dL^{-1}, [lipids] = 3 g dL^{-1}) and the vesicle without Hb encapsulation ([lipids] = 3 g dL^{-1}) suspended in saline solution and in a series of different plasma substitute solutions of rHSA, HES_{70}, and HES_{130}. In the presence of these plasma substitutes, the decay of $g_2(t)$ becomes apparently slower, indicating the induced depletion forces by plasma substitute (Figures 9a). As shown in Figure 9b, we confirmed that with no reference to Hb-encapsulation, $g_2(t)$ exhibits a similar trend.

In Figure 9c, we compare the TC-DLS result on the concentrated HbV ([Hb] = 8 g dL^{-1}) suspended in 5 g dL^{-1} rHSA solution to that of the dense stock HbV dispersion ([Hb] = 10 g dL^{-1}) in saline solution. We note that rHSA is currently a leading candidate for the coinjected plasma substitute, and most preclinical tests of the HbV were carried out using rHSA.[8,9] These two samples exhibit similar single-step behavior of $g_2(t)$ and a rapid decrease to the baseline. This observation provides evidence for ergodicity of these two samples as a nature of single fluid phase, which supports the results obtained in the previous rheological study.

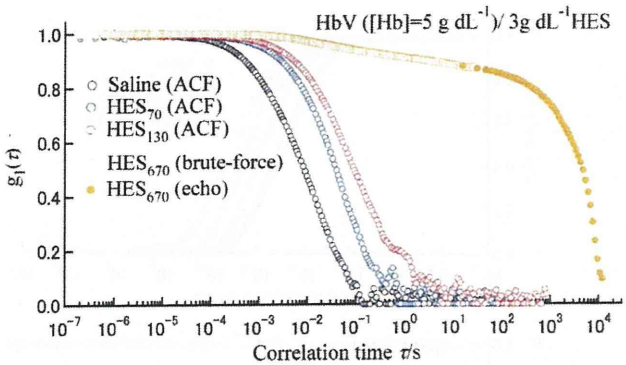

Figure 10. The field correlation functions, $g_1(t)$, of the concentrated HbV ([Hb] = 5 g dL^{-1}, [Lipids] = 3 g dL^{-1}) dispersed in saline and in a series of HES solutions. The $g_1(t)$ of the HbV/HES$_{670}$ was measured using bruteforce and echo DLS techniques in the thin layer cell configuration. The $g_1(\tau)$ data on the HbV in saline and in the lower-molecular-weight HES solutions (HES$_{70}$ and HES$_{130}$) were converted from the $g_2(t)$ data shown in Figure 9a.

Effects of Large-Molecular-Weight HES on the Particle Motions of HbV. If the HbV is suspended at [Hb] = 5 g dL^{-1} in high concentration solutions of HES$_{670}$, MFG, or DEX, the occurrence of HbV flocculation is apparent. HbV exhibits gradual sedimentation and phase separation, as an RBC does in normal blood. Note that no hemolysis was observed in these flocculating systems. To explore the arrested dynamics in the flocculating dispersion, we employed bruteforce[44] and echo DLS[43-45] experiments. The multispeckle averaging can be achieved in the bruteforce technique by step-by-step altering the sample configurations and performing repeated short time measurements. For a long-time part of (τ > 10 s), the sample cell was precisely rotated to explore many independent sample geometries during one evolution of the rotation to observe echo peaks. The time averaging can essentially be identical with the ensemble averaging.

In Figure 10, we display the field correlation function, $g_1(\tau)$, of the concentrated HbV ([Hb] = 5 g dL^{-1}, [lipids] = 3 g dL^{-1}) dispersed in a series of 3 g dL^{-1} HES solutions. The data of HbV/HES$_{670}$ dispersion were measured with the brute-force and echo DLS techniques in the TC configuration, and other $g_1(\tau)$ functions for HbV in saline and in the lower-molecular-weight HES solutions (HES$_{130}$ and HES$_{70}$) are converted from the same $g_2(\tau)$ data already shown in Figure 9a. In contrast to the rapid single-step relaxation behavior and apparently ergodic nature of the HbV/saline, HbV/HES$_{70}$, and HbV/HES$_{130}$ systems, the HbV/HES$_{670}$ dispersion shows a significant slowdown of the particle diffusion dynamics and looks like nonergodic within our time window (up to 3 × 10^4 sec). The process is characterized by the two-step behavior of $g_1(t)$, showing a faster decay with a small amplitude of ca. 0.15, and the following second slower decay. This observation demonstrates that the short-range particle diffusion is highly restricted in a flocculating system due to the depletion (polymer-induced adhesive) interaction between the HbV particles. The slower decay appears to reflect the slow dynamics of the large HbV flocculation in a HbV rich-phase of the phase separated dispersion, which certainly involves an aging effect during the echo experiment. Although we did not perform echo measurements for the HbV/DEX and HbV/MFG dispersions, repeated short-time DLS measurements with rotating the sample cell gave strong fluctuations of the intercept (coherence factor). This is a clear signature of the nonergodicity or gradual phase-separation of these samples.

Conclusions

We have investigated static structure and dynamics of HbV, a cellular-type artificial oxygen carrier functionalized as a transfusion alternative. DLS data on a diluted HbV dispersion evaluated by ORT yielded an averaged hydrodynamic diameter of 238 nm and a 20 nm standard deviation in volume distribution. The SAXS data on the vesicle for Hb encapsulation confirmed its unilamellar structure as designed, and the IFT analysis provided the thickness (ca. 5.8 nm) and internal electron density profiles of the bilayer membrane. Consistent with the DLS data, the forward SAXS intensity of the HbV dispersion exhibits a feature of polydisperse spherical particles having an averaged radius of ca. 120 nm, while its high q-part manifests the internal density fluctuations reflecting the structure of the encapsulated Hb solution. We found that the position, height, and width of static structure factor of the encapsulated Hbs are quite similar to those in bulk Hb solution at identical protein concentration. The finding demonstrates that confinement into an inner aqueous phase of the vesicle (ca. 240 nm ϕ) does not significantly affect the interparticle interaction of Hbs. TC-DLS combined with the bruteforce and echo technique enables us to overcome the interference from multiple scattering of a turbid sample and thus makes it possible to observe collective diffusion of a concentrated HbV dispersion in the presence of various plasma substitutes (water-soluble polymers used to maintain colloid osmotic pressure of blood in medical treatments) without dilution. It should also be mentioned that this technique is perfectly noninvasive, that is, no external force is applied to the system like in rheology. During the duration of these experiments, the HbV dispersions were perfectly stable. Actually, we confirmed that the dispersion stability of HbV and the oxygen binding function of encapsulated HbV were preserved for over two years at room temperature.[48] In contrast to the rapid single-step relaxation behavior and apparently ergodic nature of the HbV/saline, HbV/HES$_{70}$, and HbV/HES$_{130}$ systems, the HbV/HES$_{670}$ dispersion shows two-step behavior of $g_1(t)$, which looks like nonergodic within our time window; a faster decay with a small amplitude and the following second slower decay indicate that the short-range particle diffusion is strongly restricted in a flocculating system due to the depletion interaction between the HbV particles, while the slow mode appears to reflect the slow dynamics of the HbV flocculation in a HbV rich-phase of the phase separated dispersion. We note that as we confirmed in the previous rheological study,[32] such a HbV flocculation dissociates rapidly under a shear flow and is completely reversible.

Despite a controversy on the mechanism of liposome flocculation, our DLS results, simulated structure factor, and the phase behavior demonstrate that the underlying mechanism of the HbV flocculation in the presence of plasma substitutes is due to depletion interaction; exclusion of polymer molecules from the region closely spaced HbV particles induces an effective attractive potential between the HbVs, increasing the overall disorder of the system. At the same time, a pending question about a significantly weaker effect of rHSA on HbV flocculation and suspension viscosity enhancement than those induced by other polymers is clearly answered. This is attributed to a compact native structure of the protein, which efficiently reduces the reservoir polymer volume fraction, and thus suppresses the strength of the depletion forces. The significance of these entropically driven phenomena is highlighted by the tunable suspension rheology of HbVs using different combination of plasma substitute solutions. High viscosity fluid is occasionally advantageous for sustaining peripheral blood flow,

giving shear stress on the vascular wall to facilitate the production of vasorelaxation factors. The results are not only implicative in the fields of soft-condensed matter physics and biochemistry, but of interdisciplinary importance for a new class of forthcoming medical applications.

Acknowledgment. The authors thank Dr. Dominique Erni (Inselspital Hospital, University of Berne), Dr. Amy G. Tsai (University of San Diego), Dr. Masahiko Takaori (East Takarazuka Sato Hospital), and Dr. Koichi Kobayashi (Keio University) for their cooperation and meaningful discussions. This work was supported in part by Health Sciences Research Grants (Research on Publicly Essential Drugs and Medical Devices, H18-Soyaku-Ippan-022), from the Ministry of Health, Labour and Welfare, Japan (H.S., E.T.), Grants-in-Aid for Scientific Research from Japan Society for the Promotion of Science (B19300164) (H.S.), and Young Researchers Empowerment Project of Shinshu University (T.S.) from the Ministry of Education, Culture, Sports, Science and Technology (MEXT), Japan. M.M. and O.G. acknowledge financial support by the European Marie-Curie Research and Training Network on Arrested Matter under Grant MRTN-CT-2003-504712. The rHSA, HES_{130}, and MFG used in this study were gifts respectively from Nipro Co., Fresenius Kabi A.G., and B. Braun.

References and Notes

(1) Torchilin, V. P. *Nat. Rev. Drug Discovery* **2005**, *4*, 145–160.
(2) Izumi, Y.; Sakai, H.; Hamada, K.; Takeoka, S.; Yamahata, T.; Kato, R.; Nishide, H.; Tsuchida, E.; Kobayashi, K. *Crit. Care Med.* **1996**, *24*, 1869–1873.
(3) Sakai, H.; Takeoka, S.; Park, S. I.; Kose, T.; Nishide, H.; Izumi, Y.; Yoshizu, A.; Kobayashi, K.; Tsuchida, E. *Bioconjugate Chem.* **1997**, *8*, 23–30.
(4) Chang, T. M. *Artif. Organs* **2004**, *28*, 789–794.
(5) Djordjevich, L.; Miller, I. F. *Exp. Hematol.* **1980**, *8*, 584–592.
(6) Phillips, W. T.; Klipper, R. W.; Awasthi, V. D.; Rudolph, A. S.; Cliff, R.; Kwasiborski, V.; Goins, B. A. *J. Pharmacol. Exp. Ther.* **1999**, *288*, 665–670.
(7) Sakai, H.; Horinouchi, H.; Yamamoto, M.; Ikeda, E.; Takeoka, S.; Takaori, M.; Tsuchida, E.; Kobayashi, K. *Transfusion* **2006**, *46*, 339–347.
(8) Sakai, H.; Masada, Y.; Horinouchi, H.; Yamamoto, M.; Ikeda, E.; Takeoka, S.; Kobayashi, K.; Tsuchida, E. *Crit. Care Med.* **2004**, *32*, 539–545.
(9) Yamazaki, M.; Aeba, R.; Yozu, R.; Kobayashi, K. *Circulation* **2006**, *114*, I220–I225.
(10) Sakai, H.; Sou, K.; Horinouchi, H.; Kobayashi, K.; Tsuchida, E. *J. Intern. Med* **2008**, *263*, 4–15.
(11) Liu, X.; Miller, M. J.; Joshi, M. S.; Sadowaska-Krowicka, H.; Clark, D. A.; Lancaster, J. R., Jr. *J. Biol. Chem.* **1998**, *273*, 18709–19713.
(12) Vaughn, M. W.; Huang, K. T.; Kuo, L.; Liao, J. C. *J. Biol. Chem.* **2000**, *275*, 2342–2348.
(13) Sakai, H.; Sato, A.; Takeoka, S.; Tsuchida, E. *J. Biol. Chem.* **2008**, *283*, 1508–1517.
(14) Sakai, H.; Hara, H.; Yuasa, M.; Tsai, A. G.; Takeoka, S.; Tsuchida, E.; Intaglietta, M. *Am. J. Physiol.: Heart Circ. Physiol.* **2000**, *279*, H908–H915.
(15) Takeoka, S.; Ohgushi, T.; Terase, K.; Ohmori, T.; Tsuchida, E. *Langmuir* **1996**, *12*, 1755–1759.
(16) Takeoka, S.; Terase, K.; Sakai, H.; Yokohama, H.; Nishide, H.; Tsuchida, E. *J. Macromol. Sci., Pure Appl. Chem.* **1994**, *A31*, 97–108.
(17) Glatter, O.; Kratky, O. *Small-Angle X-ray Scattering*; Academic: London, 1982.
(18) *Neutron, X-Ray and Light Scattering*; Lindner, P., Zemb, Th., Eds.; North-Holland: Amsterdam, 1991.
(19) Peters, T. *All About Albumin: Biochemistry, Genetics, and Medical Applications*; Academic: New York, 1996.
(20) Meyuhas, D.; Nir, S.; Lichtenberg, D. *Biophys. J.* **1996**, *71*, 2602–2612.
(21) Sunamoto, J.; Iwamoto, K.; Kondo, H. *Biochem. Biophys. Res. Commun.* **1980**, *94*, 1367–1373.
(22) Otsubo, Y. *Langmuir* **1990**, *6*, 114–118.
(23) Tilcock, C. P.; Fisher, D. *Biochim. Biophys. Acta* **1982**, *688*, 645–652.
(24) Neu, B.; Meiselman, H. J. *Biophys. J.* **2002**, *83*, 2482–2490.
(25) Goto, Y.; Sakakura, S.; Hatta, M.; Sugiura, Y.; Kato, T. *Acta Anaesthesiol. Scand.* **1985**, *29*, 217–223.
(26) Asakura, S.; Oosawa, F. *J. Chem. Phys.* **1954**, *22*, 1255–1256.
(27) Asakura, S.; Oosawa, F. *J. Polym. Sci.* **1958**, *33*, 183–193.
(28) Vrij, A. *Pure Appl. Chem.* **1976**, *48*, 471–483.
(29) Bergenholtz, J.; Poon, W. C. K.; Fuchs, M. *Langmuir* **2003**, *19*, 4493–4503.
(30) Lekkerkerker, H. N. W.; Poon, W. C. K.; Pusey, P. N.; Stroobants, A.; Warren, P. B. *Europhys. Lett.* **1992**, *20*, 559–564.
(31) Ilett, S. M.; Orrock, A.; Poon, W. C. K.; Pusey, P. N. *Phys. Rev. E* **1995**, *51*, 1344–1352.
(32) Sakai, H.; Sato, A.; Takeoka, S.; Tsuchida, E. *Langmuir* **2007**, *23*, 8121–8128.
(33) Contaldo, C.; Plock, J.; Sakai, H.; Takeoka, S.; Tsuchida, E.; Leunig, M.; Banic, A.; Erni, D. *Crit. Care Med.* **2005**, *33*, 806–812.
(34) Tsai, A. G.; Acero, C.; Nance, P. R.; Cabrales, P.; Frangos, J. A.; Buerk, D. G.; Intaglietta, M. *Am. J. Physiol.: Heart Circ. Physiol.* **2005**, *288*, H1730–H1739.
(35) Tsai, A. G.; Intaglietta, M. *Biorheology* **2001**, *38*, 229–237.
(36) de Wit, C.; Schafer, C.; von Bismarck, P.; Bolz, S. S.; Pohl, U. *Pflügers Arch.* **1997**, *434*, 354–361.
(37) Kobayashi, K. *Biologicals* **2006**, *34*, 55–59.
(38) Sakai, H.; Tsai, A. G.; Kerger, H.; Park, S. I.; Takeoka, S.; Nishide, H.; Tsuchida, E.; Intaglietta, M. *J. Biomed. Mater. Res.* **1998**, *40*, 66–78.
(39) Webb, A. R.; Nash, G. B.; Dormandy, J. A.; Bennett, E. D. *Clin. Hemorheol.* **1990**, *10*, 287–296.
(40) Webb, A. R.; Barclay, S. A.; Bennett, E. D. *Intensive Care Med.* **1989**, *15*, 116–120.
(41) Traylor, R. J.; Pearl, R. G. *Anesth. Analg.* **1996**, *83*, 209–212.
(42) Medebach, M.; Moitzi, C.; Freiberger, N.; Glatter, O. *J. Colloid Interface Sci.* **2007**, *305*, 88–93.
(43) Medebach, M.; Freiberger, N.; Glatter, O. *Rev. Sci. Instrum.* **2008**, *79*, 073907. 1–12.
(44) Pham, K. N.; Egelhaaf, S. U.; Pusey, P. N.; Poon, W. C. K. *Phys. Rev. E* **2004**, *69*, 011503–1–13.
(45) Pham, K. N.; Egelhaaf, S. U.; Moussaïd, A.; Pusey, P. N. *Rev. Sci. Instrum.* **2004**, *75*, 2419–2431.
(46) Sou, K.; Naito, Y.; Endo, T.; Takeoka, S.; Tsuchida, E. *Biotechnol. Prog.* **2003**, *19*, 1547–1552.
(47) Sakai, H.; Masada, Y.; Takeoka, S.; Tsuchida, E. *J. Biochem. (Tokyo)* **2002**, *131*, 611–617.
(48) Sakai, H.; Tomiyama, K.; Sou, K.; Takeoka, S.; Tsuchida, E. *Bioconjugate Chem.* **2000**, *11*, 425–432.
(49) Orthaber, D.; Bergmann, A.; Glatter, O. *J. Appl. Crystallogr.* **2000**, *33*, 218–225.
(50) Schnablegger, H.; Glatter, O. *Appl. Opt.* **1995**, *34*, 3489–3501.
(51) Lehner, D.; Kellner, G.; Schnablegger, H.; Glatter, O. *J. Colloid Interface Sci.* **1998**, *201*, 34–47.
(52) Weyerich, B.; Brunner-Popela, J.; Glatter, O. *J. Appl. Crystallogr.* **1999**, *32*, 197–209.
(53) Fritz, G.; Bergmann, A.; Glatter, O. *J. Chem. Phys.* **2000**, *113*, 9733–9740.
(54) Fritz, G.; Glatter, O. *J. Phys.: Condens. Matter* **2006**, *18*, S2403–S2419.
(55) Koppel, D. E. *J. Chem. Phys.* **1972**, *57*, 4814–4820.
(56) Schnablegger, H.; Glatter, O. *Appl. Opt.* **1991**, *30*, 4889–4896.
(57) Frühwirth, T.; Fritz, G.; Freiberger, N.; Glatter, O. *J. Appl. Crystallogr.* **2004**, *37*, 703–710.
(58) Glatter, O. *J. Appl. Crystallogr.* **1980**, *13*, 577–584.
(59) Glatter, O. *J. Appl. Crystallogr.* **1977**, *10*, 415–421.
(60) Sou, K.; Endo, T.; Takeoka, S.; Tsuchida, E. *Bioconjugate Chem.* **2000**, *11*, 372–379.
(61) Sato, T.; Sakai, H.; Sou, K.; Buchner, R.; Tsuchida, E. *J. Phys. Chem. B* **2007**, *111*, 1393–1401.
(62) Glatter, O. *J. Appl. Crystallogr.* **1981**, *14*, 101–108.
(63) Glatter, O. *Prog. Colloid Polym. Sci.* **1991**, *84*, 46–54.
(64) Mittelbach, R.; Glatter, O. *J. Appl. Crystallogr.* **1998**, *31*, 600–608.
(65) Rodriguez, C.; Naito, N.; Kunieda, H. *Colloid Surf., A* **2001**, *237–246*, 181.
(66) Sato, T.; Komatsu, T.; Nakagawa, A.; Tsuchida, E. *Phys. Rev. Lett.* **2007**, *98* (1–4), 208101.
(67) Stradner, A.; Sedgwick, H.; Cardinaux, F.; Poon, W. C. K.; Egelhaaf, S. U.; Schurtenberger, P. *Nature* **2004**, *432*, 492–495.
(68) Liu, Y.; Chen, Fratini, E.; Baglioni, P.; W. R.; Chen, S. H. *Phys. Rev. Lett.* **2005**, *95* (1–4), 118102.
(69) Stradner, A.; Thurston, G. M.; Schurtenberger, P. *J. Phys.: Condens. Matter* **2005**, *17*, S2805–S2816.
(70) Chihara, J. *Prog. Theor. Phys.* **1973**, *50*, 409–423.
(71) Madden, W. G.; Rice, S. A. *J. Chem. Phys.* **1980**, *72*, 4208–4215.

JP9002142

Am J Physiol Heart Circ Physiol 297: H583–H589, 2009.
First published June 5, 2009; doi:10.1152/ajpheart.00352.2009.

Peculiar flow patterns of RBCs suspended in viscous fluids and perfused through a narrow tube (25 μm)

Hiromi Sakai,[1] Atsushi Sato,[2] Naoto Okuda,[2] Shinji Takeoka,[2] Nobuji Maeda,[3] and Eishun Tsuchida[1]

[1]*Research Institute for Science and Engineering, Waseda University, and* [2]*Department of Life Science and Medical Bioscience, Graduate School of Science and Engineering, Waseda University, Tokyo; and* [3]*Department of Physiology, School of Medicine, Ehime University, Ehime, Japan*

Submitted 10 April 2009; accepted in final form 5 June 2009

Sakai H, Sato A, Okuda N, Takeoka S, Maeda N, Tsuchida E. Peculiar flow patterns of RBCs suspended in viscous fluids and perfused through a narrow tube (25 μm). *Am J Physiol Heart Circ Physiol* 297: H583–H589, 2009. First published June 5, 2009; doi:10.1152/ajpheart.00352.2009.—Red blood cells (RBCs) generally deform to adopt a parachute-like, torpedo-like, or other configuration to align and flow through a capillary that is narrower than their major axis. As described herein, even in a narrow tube (25 μm) with diameter much larger than that of a capillary, flowing RBCs at 1 mm/s align axially and deform to a paraboloid shape in a viscous Newtonian fluid (505 kDa dextran medium) with viscosity of 23.4–57.1 mPa·s. A high-speed digital camera image showed that the silhouette of the tip of RBCs fits a parabola, unlike the shape of RBCs in capillaries, because of the longer distance of the RBC-free layer between the tube wall and the RBC surface (~8.8 μm). However, when RBCs are suspended in a "non-Newtonian" viscous fluid (liposome-40 kDa dextran medium) with a shear-thinning profile, they migrate toward the tube wall to avoid the axial lining, as "near-wall-excess," which is usually observed for platelets. This migration results from the presence of flocculated liposomes at the tube center. In contrast, such near-wall excess was not observed when RBCs were suspended in a nearly Newtonian liposome-albumin medium. Such unusual flow patterns of RBCs would be explainable by the principle; a larger particle tends to flow near the centerline, and a small one tends to go to the wall to flow with least resistance. However, we visualized for the first time the complete axial aligning and near-wall excess of RBCs in the noncapillary size tube in some extreme conditions.

hemorheology; erythrocytes; viscometry; artificial red cells; microcirculation

RED BLOOD CELLS (RBCs) or erythrocytes in mammals lost their nuclei during their evolution and specialization for their role of oxygen transport. Microcirculatory observation of capillaries (>4 μm diameter) that are narrower than the RBC diameter (8 μm) revealed that flowing RBCs alter their own morphology from a biconcave disk to various configurations resembling a parachute, umbrella, jellyfish, or torpedo, as though they were alive (10, 11, 29). This phenomenon was first reported in the 1960s.

During blood flow in a capillary, a pressure gradient exists: a pressure drop in the direction of flow. The higher pressure in the rear tends to compress the rear portion of the RBCs. In response to such stress, the elastic cellular structure of RBCs (biconcave disc) is known to be effective to deform and stir the intracellular viscous hemoglobin (Hb) solution (>35 g/dl), thereby facilitating gas exchange (1, 6, 14). From conventional microscopic observation of peripheral tissues, it is difficult to discern the capillary shape, especially at a reduced hematocrit resulting from the Fahraeus effect and plasma skimming, but we can infer the presence of functional capillary walls near the RBCs by the presence of deformed and aligned RBC flow (25, 29). In glass tubes (inner diameter, <12 μm), similar deformation of RBCs is apparent (8, 35). On the other hand, the glycocalyx layer of the capillary endothelium interacts with the plasma layer fluid and retards its flow. Its hydraulic resistance narrows the lubrication layer and enhances velocity gradients in glycocalyx-layered capillaries compared with glass tubes of the same diameter. The narrower lubrication layers and greater shear stress on the RBC surface give rise to greater pressure gradients in the gap and larger tensions on the RBC membrane surface. Consequently, RBCs experience a higher state of stress and undergo greater deformation in capillaries lined with a glycocalyx (5, 27). The distance between the surface of RBCs and the capillary wall is expected to be <0.5 μm.

As described herein, we examined the flow patterns of RBCs in a non-capillary-sized tube (25 μm diameter) where the distance between RBC and the tube wall is much greater than that in capillaries and where RBCs were suspended in Newtonian and non-Newtonian viscous fluids. We discovered peculiar flow patterns of RBCs being subjected to least resistance in some extreme conditions.

MATERIALS AND METHODS

Preparation of suspending solutions and their viscometric analyses. We prepared Newtonian fluids using dextran (Dex) and non-Newtonian fluids using liposomes for suspending RBCs.

A high-molecular-mass Dex (mol mass 505 kDa) was purchased from Sigma-Aldrich. This is dissolved in a normal saline solution (0.9% NaCl; Otsuka Pharmaceutical) at concentrations of 0–15 g/dl to prepare Dex solutions of various viscosities. Physiological Dex solution (mol mass 40 kDa, 10% solution in saline) was purchased from Kobayashi Pharmaceutical. Steady-shear viscosity measurements were taken using a rheometer (Physica MCR 301; Anton Paar, Graz, Austria). The viscosity increases concomitantly with increasing concentration of Dex. However, they are all Newtonian because the viscosities are fundamentally identical at all shear rates (Table 1 and Fig. 1).

A high-concentration liposomal suspension was prepared from a mixture of 1,2-dipalmitoyl-*sn*-glycero-3-phosphatidylcholine, cholesterol, and 1,5-bis-*O*-hexadecyl-*N*-succinyl-L-glutamate in a molar ratio of 5:5:1 (Nippon Fine Chemical, Osaka, Japan) and 1,2-distearoyl-*sn*-glycero-3-phosphatidylethanolamine-*N*-poly(ethylene glycol) (0.3 mol% of the total lipid; NOF, Tokyo, Japan) (21, 22). The particle size was regulated using an extrusion method and suspended in physiological saline; the resultant particle diameter was 279 ± 95 nm. The liposomes contained a concentrated human Hb solution (35 g/dl) (21, 22). The resulting liposomal suspension was once ultracentrifuged

Address for reprint requests and other correspondence: H. Sakai, Research Institute for Science and Engineering, Waseda Univ., 3-4-1 Okubo, Shinjuku, Tokyo 169-8555, Japan (e-mail: hiromi@waseda.jp).

Table 1. *Viscosity of Newtonian dextran solutions used for the suspending media and the flow conditions*

Image in Fig. 2	Mol mass of Dex, kDa	[Dex], g/dl	Viscosity at 25°C, mPa·s			Applied Pressure for Perfusion, kPa	Shear Stress on the Tube Wall at a Shear Rate of 160 s^{-1}, dyn/cm^2
			At 10 s^{-1}	At 160 s^{-1}	At 1,000 s^{-1}		
A	[a]	0.0	1.0	0.9	0.9	5.5	2
B	40	10.0	4.5	4.5	4.5	23	7
C	505	5.0	7.1	7.0	7.0	39	11
D	505	7.0	13.3	13.2	13.2	63	21
E	505	8.0	15.1	15.0	14.9	78	24
F	505	8.4	16.5	16.4	16.4	90	26
G	505	10.0	23.7	23.4	23.4	110	37
H	505	15.0	57.7	57.4	57.1	280	91

Dex, dextran; [Dex], dextran concentration. [a]Normal saline solution.

(50,000 *g*, 30 min) and resuspended in 5% recombinant human serum albumin, obtained from Nipro. The concentrations of lipids and Hb were adjusted, respectively, to 6 and 10 g/dl. The resulting liposome-albumin suspensions were nearly Newtonian, as shown by similar viscosities 5.9 and 3.9 mPa·s, respectively, at shear rates of 10^{-1} and 1,000 s^{-1}, although the volume of occupancy by liposomes is as high as 40 vol% (22) (Table 2, Fig. 1). Similarly, the liposome was resuspended in 4 g/dl Dex solution (mol mass 40 kDa, 10 g/dl; Kobayashi Pharmaceutical) to prepare a non-Newtonian viscous suspension, as shown respectively by significantly different viscosities 95.7 and 16.2 mPa·s at shear rates of 10^{-1} and 1,000 s^{-1}. A so-called "shear-thinning" profile results from the dissociation of flocculated liposomes at a higher shear rate (22). Because of the red color of the flocculated Hb-containing liposomes in 40 kDa Dex, the flowing RBCs are not clearly observed. To solve the problem, we prepared liposomes without the intraliposomal Hb at the identical lipid concentration (6 g/dl). The absence of Hb does not affect the resulting suspension rheology.

Preparation of human RBC suspensions. In this study we used flesh human blood specimens. The study was approved by the Ethical Committee of Waseda University on medical research involving human subjects and performed according to the World Medical Association Declaration of Helsinki and Title 45, U.S. Code of Federal Regulations, Part 46, Protection of Human Subjects (Revised November 13, 2001). After obtaining the written informed consents from A. Sato and N. Okuda, a blood specimen was withdrawn and was heparinized and washed two times using two cycles of gentle centrifugation and resuspension in saline. Subsequently, the RBCs were permeated through a filter for leukocyte removal (Pall leukocyte removal filter RC NE01J; Kawasumi Laboratories). Finally, the Hb concentration of the RBC suspension was adjusted to 10 g/dl (hematocrit = ~30%). The obtained RBC suspension was mixed with the test-suspending solutions (40 kDa, 505 kDa Dex solutions, liposome-albumin, liposome-40 kDa Dex, saline) at the volume ratio of 1:19. Consequently, the Hb concentration was 0.5 g/dl. Next, hematocrit was ~1.5%.

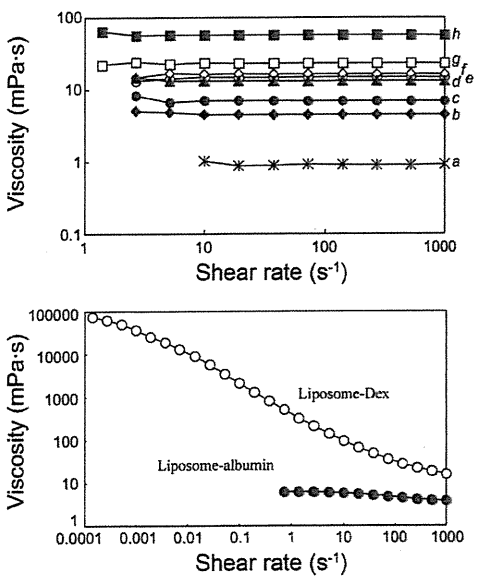

Fig. 1. Shear rate dependence of the viscosity of the suspending media for red blood cells (RBCs) at 25°C. *Top*: viscosities of all dextran (Dex) solutions are fundamentally independent of the shear rate, indicating that they are Newtonian (*a–h*, see Fig. 1 and Table 1). *Bottom*: liposome-40 kDa Dex showed a marked "shear-thinning profile" as a typical non-Newtonian fluid. In contrast, the liposome-albumin is almost Newtonian. The viscosity of liposome-40 kDa Dex is measurable at a lower shear rate because of a sufficiently high strain of detection. The low-viscosity fluids were measurable only above 1 s^{-1}.

Flow experiment using a narrow artificial tube. Narrow tubes (inner diameter, 25 μm; wall thickness, 37.5 μm; length, 150 mm) were produced from a fluorinated ethylenepropylene copolymer at Hirakawa Hewtech (Ibaraki, Japan) (15, 24, 31). One end of the narrow tube was connected to a reservoir of the RBC suspensions. The entrance of the tube protruded into the suspension. The tube was placed horizontally on the stage of an inverted microscope (IX71; Olympus) with an objective lens of ×40 magnification (LCPlanFl; Olympus). The suspension in the reservoir was mixed gently and continuously using a small magnetic stirrer (CC 301; AS One); it was then pressurized using a syringe connected to a syringe pump (FP-W-100; Toyo Sangyo). The perfusion pressure was monitored using a digital pressure sensor (AP-C30; Keyence). The centerline RBC flow velocity was analyzed using photodiodes and the cross-correlation technique (Velocity Tracker Mod-102 B; IPM) (12); it was adjusted to 1 mm/s by changing the pressure that was applied to the reservoir. Under these conditions, the shear rate at the tube wall was 160 s^{-1}, Reynolds numbers were 0.00044 for the most viscous Dex solution and 0.025 for the saline solution. The laminar flow was established theoretically. These values are comparable with values reported for human capillaries (34). In our experiments, the hematocrit of the suspension was adjusted to only 1.5%, and the influence of RBCs on the Newtonian profile and the laminar flow would be minimal. A measuring spot on the narrow tube was at the middle of the tube length. The visual field of the microscope was fixed on a monitor (PVM-14L2; Sony) through a CCD camera (DXC-930; Sony). The images of RBCs were recorded using a DVD recorder (DMR-E95H; Panasonic). The entire perfusion experiment was performed at 25°C. In this study, we defined the RBC-free layer thickness as the distance between the tube inner wall and the edge of a nearest RBC. This parameter is usually used for a concentrated RBC flow; however, we think it is the most appropriate parameter to show the high level of centralization in the narrow tube. The RBC-free layer thickness was measured at 10 points using an image-processing technique. When RBCs were suspended in the liposome-40 kDa Dex solution, the

Table 2. *Viscosity of the liposome-polymer mixed fluids used for the suspending media*

Image in Fig. 6	Liposome-Polymer Mixed Fluid	[Polymer], g/dl	Viscosity at 25°C, mPa·s			Applied Pressure for Perfusion, kPa
			At 10 s^{-1}	At 160 s^{-1}	At 1,000 s^{-1}	
A	Liposome-40 kDa Dex	10	95.7	27.8	16.2	19
B	Liposome-albumin	5	5.9	4.4	3.9	7

The total lipid concentration of the liposome suspension was 6 g/dl, and the liposomes contained a 35 g/dl purified hemoglobin solution. [Polymer], polymer concentration.

distances from the tube inner wall to the nearest and the farthest edges of the RBCs were measured at 25 points similarly. The values were averaged and expressed as means ± SD.

For detailed analyses of the flowing RBCs' shape, images of RBCs suspended in the most viscous 505-kDa Dex solution were recorded using a high-speed digital imaging camera (Phantom Miro 4M; Vision Research, Wayne, NJ) with an objective lens of ×100 magnification (UPlanApo; Olympus). The capturing frame interval was 1 ms; the exposure time was 0.2 ms. The RBC shape was compared with a theoretical parabolic velocity distribution of a Newtonian fluid of laminar flow.

For a statistical analysis, seven images of RBCs flowing individually or at the top in a group in the most viscous 505-kDa Dex solution were randomly selected and magnified on a monitor. The silhouette were sketched and digitalized by UN-SCAN-IT (Silk Scientific, Orem, UT). The data were plotted, and an approximate curve of the second order was obtained by a least-square method using Excel 2004 for Mac (Microsoft).

RESULTS

Flow patterns of RBCs suspended in viscous Newtonian fluid. When RBCs were suspended in a normal saline aqueous solution (viscosity = 0.9 mPa·s) or a 40 kDa Dex solution (10% solution, 4.5 mPa·s) and perfused through the narrow tube at the centerline RBC flow velocity of 1 mm/s, a tendency of centralization was observed, although the RBCs retained a biconcave disk form (Fig. 2, *A* and *B*).

We dissolved a high-molecular-mas Dex (mol mass 505 kDa) to increase the viscosity of the suspending saline medium. Figure 1 and Table 1 show that the resulting 505-kDa Dex solutions are thereby viscous Newtonian fluids. The applied pressure for perfusion reached 280 kPa. The estimated shear stress on the tube wall reached 91 dyn/cm^2 at a shear rate of 160 s^{-1}. With increased viscosity of the suspending medium of RBCs up to 57.1 mPa·s, it enhanced centralization (Fig. 2, *C–H*). As a result, the RBC-free layer (peripheral fluid layer) thickness increased and reached a plateau of ~8.8 μm (Fig. 3). The RBCs flowed axially and deform to an axisymmetrical paraboloidal shape when the viscosity was increased to 16.7, 23.4, and 57.1 mPa·s (Fig. 2, *F–H*) [see Supplemental Movies S1 (Supplemental material for this article may be found on the *American Journal of Physiology: Heart and Circulatory Physiology* website.)].

The flowing profile of RBCs in the most viscous Dex suspension was observed using a high-speed digital imaging camera (Phantom Miro 4) (Fig. 4*A*). The picture clearly illustrates the nearly axisymmetrical paraboloidal formation (see Supplemental Movies S2). The skirt hem of RBCs become semi-transparent, and the tip of the following RBC is visible through the hem (for example, the second, the third, and the last RBC).

The red plotted curve portrays a paraboloidal curve imaging a velocity (v) distribution in an arbitrary unit: $v = a[1 - (r^2/r_o^2)]$, where a is the centerline velocity, r is the distance from the centerline, and r_o is the radius of the tube, showing that v at the centerline is the fastest, and it becomes zero at the wall under the assumption of a rectilinear laminar flow of a viscous, incompressible, Newtonian fluid. The silhouette of the tip of RBCs seems coinciding well with a paraboloidal curve. On the other hand, the simulated shape of a RBC flowing in a capillary (diameter, ~8.2 μm) (30) shows that the silhouette of the tip of an RBC is rather blunted compared with the paraboloidal curve (Fig. 4*B*). In a narrower capillary, an RBC deforms to a torpedo-like configuration (27); its silhouette does not resemble the paraboloidal curve (Fig. 4*C*). For a detailed analysis the shape of RBCs, seven images of the silhouettes are digitalized

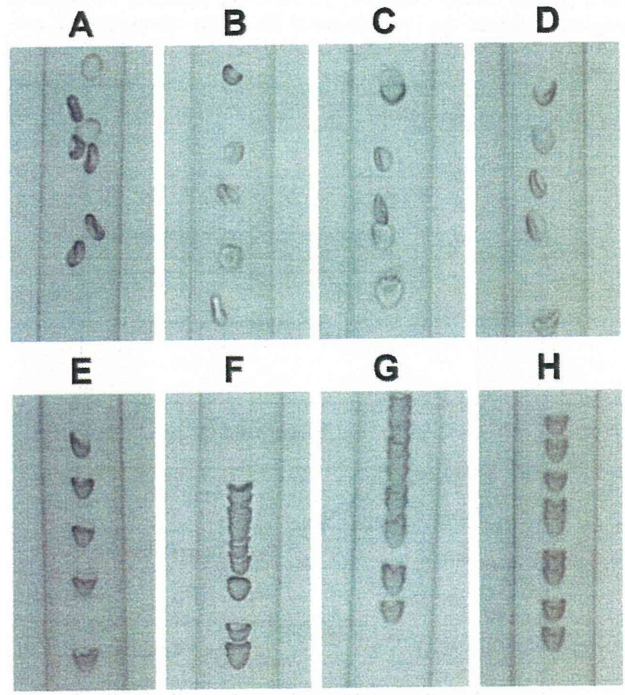

Fig. 2. Optical microscopic views of the flow patterns of RBCs suspended in different-viscosity Newtonian solutions in the tube (inner diameter, 25 μm). The solutions' viscosities were regulated by dissolving Dex (mol mass 505 kDa) (*A–G*). Viscosity (mPa·s) at 1,000 s^{-1}: 0.9 (*A*), 4.5 (*B*), 7.0 (*C*), 13.2 (*D*), 14.9 (*E*), 16.7 (*F*), 23.4 (*G*), and 57.1 (*H*). Complete alignment of RBCs becomes evident with increased viscosity of the suspending medium to 23 and 57 mPa·s (*F–H*). A representative movie is available in Supplemental Movie S1. The RBCs are deformed to an axisymmetrical paraboloidal shape. In this condition, RBCs tended to flow in groups. Hemoglobin (Hb) concentration = 0.5 g /dl, hematocrit = 1.5%.

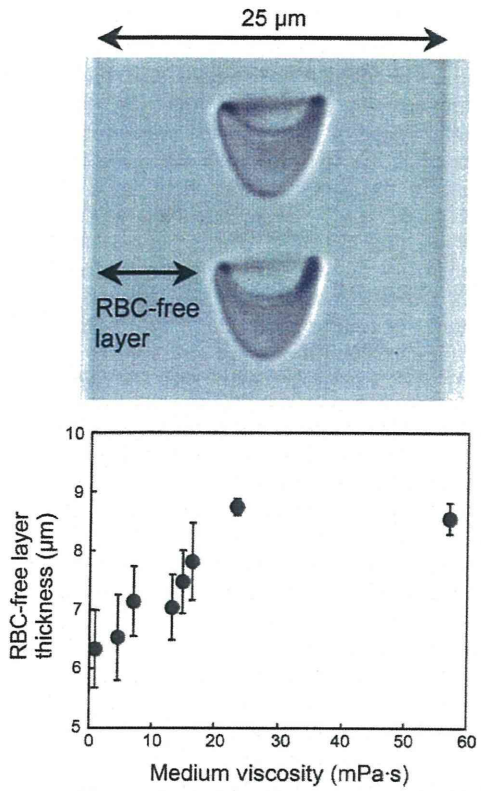

Fig. 3. Thickness of the RBC-free layer (peripheral fluid layer) when RBCs are flowing in narrow tubes. *Top*: image of axisymmetrical paraboloidal formation of RBCs taken using a high-speed digital imaging camera (Phantom Miro 4) and the definition of the thickness of the RBC free layer. *Bottom*: thickness of RBC-free layer increased from 6.2 to 8.7 μm on average, and reached a plateau >23 mPa·s. Mean ± SD (n = 10 experiments).

and plotted as shown in Fig. 5. The approximate curve of the second order is obtained by the least mean-square method as follows: $y = 0.4283x^2 + 0.0509x - 0.2329$ (determination coefficient: $r^2 = 0.958$). The curve is slightly tilted, and the equation contains a primary expression with little influence to the curve of the second order.

Flow patterns of RBCs suspended in viscous non-Newtonian fluid. When RBCs were suspended in the liposome-40 kDa-Dex fluid and perfused through the narrow tube, the RBCs tended to show "near-wall excess" as portrayed in Fig. 6*A*. On the other hand, when RBCs were suspended in the liposome-albumin fluid, neither near-wall excess nor axial lining was observed. However, RBCs tended to show centralization (Fig. 6*B*). Because of the encapsulated Hb and homogeneous distribution of liposomes in albumin solution, the tube is homogeneously blackened. On the other hand, the liposomes were flocculated in 40 kDa Dex solution; the background is heterogeneous. To more clearly show the near-wall excess, we additionally prepared liposomes that do not contain Hb. RBCs were suspended in the liposome (without Hb)-40 kDa-Dex fluid and perfused through the tube in the same condition. The near-wall excess of RBCs was more clearly visualized (Fig. 6, *C* and *D*). The shape of RBCs was nearly biconcave but slightly stretched. The distances from the tube inner wall to the nearest and farthest edges of RBCs were 2.7 ± 0.9 and 7.6 ± 1.4 μm, respectively. In Fig. 6*D*, the round shape of the RBCs near the back side of the tube wall becomes unclear because of the semi-transparency of the suspending medium by the presence of flocculated liposomes in the center of the tube.

DISCUSSION

Our principal finding in this study is that, even in a plastic tube (inner diameter, 25 μm) much larger than a capillary, the flowing human RBCs deform to a completely symmetric paraboloidal formation and align axially when RBCs are suspended in an extremely viscous Newtonian fluid. However, when RBCs are suspended in a viscous non-Newtonian fluid with a shear-thinning profile, they flow near the wall, avoiding centralization, as near-wall excess for platelets (33).

Centralization of RBCs in a normal saline aqueous solution and 40 kDa Dex solution was observed at the centerline RBC flow velocity of 1 mm/s, although the RBCs retained a biconcave disk form. This situation is often observed in microvessels

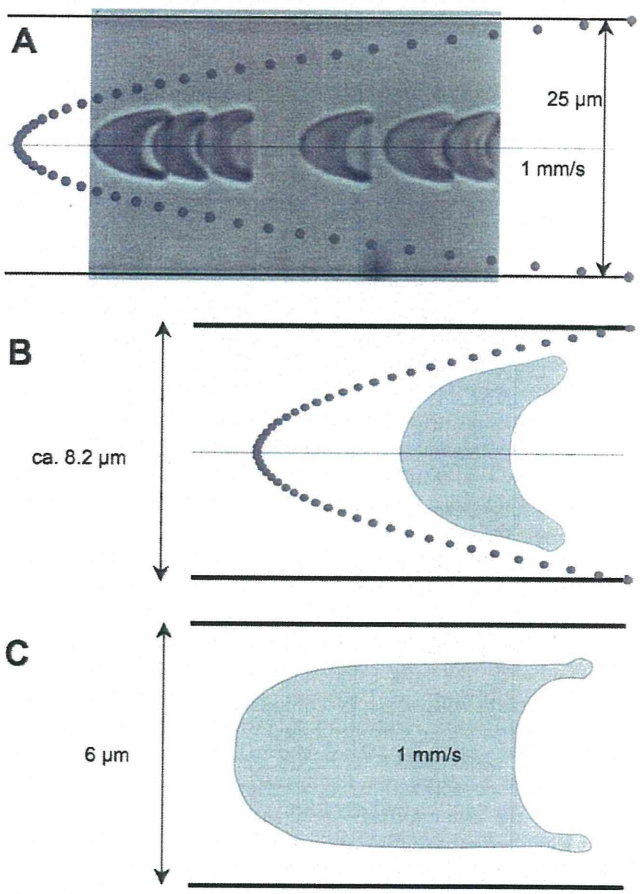

Fig. 4. *A*: magnified view of the flowing RBCs suspended in the most viscous Dex solution (57 mPa·s) taken using a high-speed digital imaging camera. The centerline velocity was 1 mm/s. A slow-motion movie is available as Supplemental Movie S2. The red plots portray an arbitrary paraboloidal curve, imaging an example of velocity distribution of a rectilinear laminar flow of a viscous, incompressible, Newtonian fluid. The silhouette of the tip of RBCs coincides well with the paraboloidal curve. Simulated shape of a RBC flowing in a capillary (diameter, ca. 8.2 μm) (30) (*B*), and a torpedo-like configuration in a narrower capillary (27) are shown for comparison (*C*).

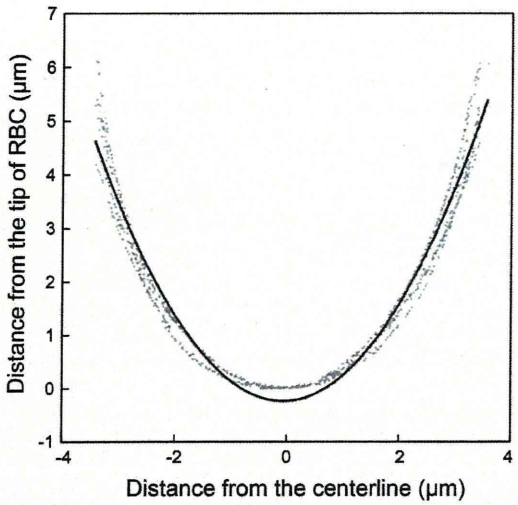

Fig. 5. The silhouettes of RBCs (n = 7, gray narrow lines) flowing through narrow capillaries when RBCs were suspended in the most viscous Dex solution (57 mPa·s). The approximate curve of the second order (black line) is obtained by the least mean-square method as: $y = 0.4283x^2 + 0.0509x - 0.2329$ (determination coefficient: $r^2 = 0.958$).

such as venules after extreme hemodilution and in ex vivo microtube flow experiments (9, 17). Increased viscosity of the suspending medium of RBCs up to 57 mPa·s enhances centralization. The RBCs flow axially and deform to an axisymmetrical paraboloidal shape, thereby increasing the thickness of the RBC-free layer (peripheral fluid layer). The RBCs tended to flow in groups rather than assume an equally spaced arrangement (8), presumably *1*) because a vortex motion of the intercellular viscous fluid facilitates the access of the neighboring RBC or *2*) because of Dex-induced RBC aggregation in the reservoir before perfusion through the tube (19). The flowing RBCs in the most viscous Dex suspension were observed using a high-speed digital imaging camera. The image clearly depicts the axisymmetrical paraboloidal formation. The rear edge of RBCs (the skirt hem) becomes so thin and semi-transparent that the tip of the following RBC is visible through the hem.

Reportedly, intravenous injection of a high-molecular-mass Dex induces RBC aggregation and increases the RBC-free layer thickness (2, 19, 31). Under a simple and strong shear stress induced by suspension in viscous fluid and a cone plate viscometer, the tank-tread motion and deformation of RBCs into prolate ellipsoids is enhanced (7, 26). Contrary to the asymmetric shear stress induced by a cone plate, our axisymmetrical shear stress to RBCs shows for the first time the complete centralization, axial aligning, and parabolic formation in the non-capillary-sized tube.

Rheological conditions in this study differ extremely from the physiological condition. Irrespective of the viscosity, the flow velocity and shear stress of all the Newtonian fluids are expected to be axisymmetrical in the tube with a smooth wall. The low hematocrit of the suspension, only 1.5%, would not influence on the parabolic velocity field significantly. The shear rate at the tube wall was ~160 s^{-1}. The shear stress on the wall when complete centralization, axial aligning, and parabolic formation appeared was as high as 24–91 dyn/cm^2 (cf. arteriolar capillaries <20 dyn/cm^2). To avoid such high stress, the RBCs migrate toward the tube center by the difference of shear stress in a parabolic velocity field. The low hematocrit facilitated a single-file flow (complete axial aligning) rather than a multifile flow (8). Compared with the parabolic shape of RBCs in the present study, the simulated shapes of RBCs in capillaries are more blunted (5, 27, 30) because of the short distance between a capillary wall and RBCs (ca. 0.5 μm). The statistical analysis of the silhouettes of RBCs provided the approximate curve of the second order as shown in Fig. 5, with a high determination coefficient (r^2 = 0.958), indicating mathematically that the shape of RBCs in this study is nearly parabolic. This might be related to the parabolic distribution of shear stress in the tube. However, the front of RBCs does not seem actually parabolic in shape. A more-detailed mathematical analysis would be needed to clarify the relationship between the shape of parabolic RBCs and the physical condition of both the suspending medium and the counteracting RBC membrane (35).

Contrary to the feature of centralization, RBCs showed a near-wall excess when they were suspended in a viscous non-Newtonian fluid, as is usually observed for platelets in microcirculation (33). The distance from the tube inner wall and the nearest RBC became only 2.7 ± 0.9 μm, which was much shorter than the RBC-free layer in Fig. 2 when RBCs were suspended in normal saline (6.3 ± 0.7 μm). The distance from the wall to the farthest edges of RBCs was 7.6 ± 1.4 μm, indicating the formation of RBC-free zone in the center of the tube of ~9.8 μm in diameter (= 25 − 2 × 7.6). As the non-Newtonian fluid, we used a concentrated liposome suspension mixed with a 40 kDa Dex solution. The occupied volume fraction of liposome is nearly 40%, and the fluid shows a "shear-thinning" profile because the liposome flocculation reversibly dissociates at a higher shear rate. At the center of the tube, where the shear rate is the lowest, viscosity is extremely high because of the presence of fractal-structured flocculation of liposomes (22). The parabolic velocity profile in a tube would become slightly blunted because of the presence of the

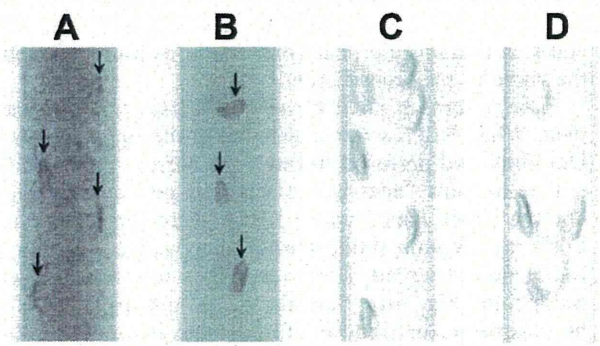

Fig. 6. Optical microscopic views of the flow patterns of RBCs suspended in liposomal suspensions in the tube (inner diameter, 25 μm). *A*: RBCs were suspended in a non-Newtonian viscous fluid (liposome-40 kDa Dex). The RBCs tended to flow near the tube wall, as shown by the arrows. *B*: RBCs were suspended in a nearly Newtonian viscous fluid (liposome-albumin). The RBCs tended to flow near the centerline, but they are not aligned completely, as were RBCs suspended in saline (Fig. 2*A*). The liposomes encapsulated concentrated Hb solutions (Hb-vesicles). Therefore, the suspension background is darkened in black and white compared with conditions presented in Fig. 2. (*C*, *D*). RBCs were suspended in the liposome (without Hb)-40 kDa-Dex fluid and perfused through the tube in the same condition. The near-wall excess of RBCs was more clearly visualized.

liposome flocculation (2), which increases the shear rate near the wall where the flocculation tends to be dissociated. In such a condition, RBCs are excluded by flocculation and migrate to the near-wall location, where the viscosity is expected to be lowest and where RBCs can move more freely. In principle, the above phenomena are explainable by the size of particles; a larger particle tends to flow near the centerline (4, 13). For comparison, RBCs were suspended in a nearly Newtonian liposomal suspension suspended in 5% albumin solution to confirm whether the occupied volume fraction of liposome (40%) influences the flow profiles. In this case, liposomes were dispersed homogeneously in the tube, and RBCs showed centralization without axial alignment. The RBCs showed no near-wall excess (Fig. 6*B*). At this condition, the viscosity of the suspending medium, 3.9–5.9 cP, and the viscosity of 40 kDa Dex (Fig. 2*B*), 4.5 cP, are similar, and the RBC flow patterns are also similar.

In fact, such a highly concentrated liposomal suspension is used for liposome-encapsulated Hb as the artificial oxygen carrier (Hb vesicles) (21, 23) that we have studied extensively for use as a transfusion alternative. Results of this study demonstrate that homogeneously dispersed Hb vesicles would not influence the flow pattern of RBCs in microcirculation. A considerable amount of oxygen is known to be released from RBCs at a microvessel level. The narrow tube comprises a gas-permeable polymeric material. Therefore, the present technique might be useful for the evaluation of artificial oxygen carriers from the standpoint of oxygen release from peripheral vessels: namely small particles of artificial oxygen carriers flow near the wall or not (24, 31). In this sense the tube diameter, 25 μm, is appropriate because it is close to the diameter of arterioles that regulates blood flow in response to the oxygen transfer.

Recently, microfluidic chips have been studied extensively for mixing small quantities of solutions, chemical reactions, separation of RBCs, cell sorters, etc., because of the easy fabrication of chips using recent advanced photoresist technologies (16, 28, 32). Most studies have specifically explored the design of the path and valve and the flow rate of the solutions. Although our experiment does not correlate directly to a microfluidic chip, the results suggest that the use of a viscous fluid might improve the efficiency for cell separation by enhancing the axial alignment and plasma skimming or near-wall excess in reverse.

The impairment of RBC deformability is well noted for metabolic and systemic complications associated with diabetes, sepsis, sickle cell anemia, etc. (14, 28). The level of axial lining of RBCs in a Newtonian viscous fluid is expected to depend not only on the rheological property of the suspending medium but also on the RBC membrane deformability. Therefore, our system could possibly be applied for analyses of abnormal RBCs.

Regarding in vivo blood circulation, once Hb is released from the RBCs in pathological conditions and after administration of cell-free Hb-based blood substitutes, the Hb induces various side effects (3, 18, 20). In our study, the ability of RBCs to find "easier" paths seems strengthened in extreme conditions to incur minimal stress. This is an important aspect of the cellular structure of RBCs to be designed to avoid hemolysis and to retain toxic Hb molecules.

Collectively, our observations are explainable by the principle; a larger particle tends to flow centerline. However, as far as we know, this is the first time to visualize such unique flow properties of RBCs in some extreme conditions, complete axisymmetrical alignment, and near-wall excess, in the narrow tube with the diameter much larger than the capillaries.

ACKNOWLEDGMENTS

We thank Dr. Koichi Kobayashi and Dr. Hirohisa Horinouchi (Keio University) for discussion.

Current address of A. Sato: NOF Corporation, Tokyo 150-6019, Japan.

GRANTS

This work is supported by Health and Labor Sciences Research Grants (Health Science Research Including Drug Innovation), Ministry of Health, Labor and Welfare, Japan (H. Sakai, E. Tsuchida), and Grants-in-Aid for Scientific Research from the Japan Society for the Promotion of Science (B19300164) (H. Sakai).

DISCLOSURES

The recombinant albumin was provided by Nipro (Osaka). H. Sakai, S. Takeoka, and E. Tsuchida are holders of patents on the liposomes (Hb-vesicles).

REFERENCES

1. **Bagge U, Brånemark PI, Karlsson R, Skalak R.** Three-dimensional observations of red blood cell deformation in capillaries. *Blood Cells* 6: 231–239, 1980.
2. **Bishop JJ, Nance PR, Popel AS, Intaglietta M, Johnson PC.** Effect of erythrocyte aggregation on velocity profiles in venules. *Am J Physiol Heart Circ Physiol* 280: H222–H236, 2001.
3. **Chang TM.** Hemoglobin-based red blood cell substitutes. *Artif Organs* 28: 789–794, 2004.
4. **Chien S, Usami S, Skalak R.** Blood flow in small tubes. In: *Handbook of Physiology. The Cardiovascular System. Microcirculation.* Bethesda, MD: Am Physiol Soc, 1984, sect. 2, vol. IV, p. 217–249.
5. **Damiano ER.** The effect of the endothelial-cell glycocalyx on the motion of red blood cells through capillaries. *Microvasc Res* 55: 77–91, 1998.
6. **Discher DE, Mohandas N, Evans EA.** Molecular maps of red cell deformation: hidden elasticity and in situ connectivity. *Science* 266: 1032–1035, 1994.
7. **Fischer TM.** Tank-tread frequency of the red cell membrane: dependence on the viscosity of the suspending medium. *Biophys J* 93: 2553–2561, 2007.
8. **Gaehtgens P, Dührssen C, Albrecht KH.** Motion, deformation, and interaction of blood cells and plasma during flow through narrow capillary tubes. *Blood Cells* 6: 799–817, 1980.
9. **Goldsmith HL.** Red cell motions and wall interactions in tube flow. *Fed Proc* 30: 1578–1590, 1971.
10. **Gregersen MI, Bryant CA, Hammerle WE, Usami S, Chien S.** Flow characteristics of human erythrocytes through polycarbonate sieves. *Science* 157: 825–827, 1967.
11. **Guest MM, Bond TP, Cooper RG, Derrick JR.** Red blood cells: change in shape in capillaries. *Science* 142: 1319–1321, 1963.
12. **Intaglietta M, Silverman NR, Tompkins WR.** Capillary flow velocity measurements in vivo and in situ by television methods. *Microvasc Res* 10: 165–179, 1975.
13. **Karnis A, Goldsmith HL, Mason SG.** Axial migration of particles in Poiseuille flow. *Nature* 200: 159–160, 1963.
14. **Kon K, Maeda N, Shiga T.** Erythrocyte deformation in shear flow: influences of internal viscosity, membrane stiffness and hematocrit. *Blood* 69: 727–734, 1987.
15. **Kubota K, Tamura J, Shirakura T, Kimura M, Yamanaka K, Isozaki T, Nishio I.** The behaviour of red cells in narrow tubes in vitro as a model of the microcirculation. *Br J Haematol* 94: 266–72, 1996.
16. **Laurell T, Petersson F, Nilsson A.** Chip integrated strategies for acoustic separation and manipulation of cells and particles. *Chem Soc Rev* 36: 492–506, 2007.
17. **Munn LL, Dupin MM.** Blood cell interactions and segregation in flow. *Ann Biomed Eng* 36: 534–544, 2008.

18. **Natanson C, Kern SJ, Lurie P, Banks SM, Wolfe SM.** Cell-free hemoglobin-based blood substitutes and risk of myocardial infarction and death: a meta-analysis. *JAMA* 299: 2304–2312, 2008.
19. **Neu B, Meiselman HJ.** Depletion-mediated red blood cell aggregation in polymer solutions. *Biophys J* 83: 2482–2490, 2002.
20. **Reiter CD, Wang X, Tanus-Santos JE, Hogg N, Cannon RO 3rd, Schechter AN, Gladwin MT.** Cell-free hemoglobin limits nitric oxide bioavailability in sickle-cell disease. *Nat Med* 8: 1383–1389, 2002.
21. **Sakai H, Sato A, Masuda K, Takeoka S, Tsuchida E.** Encapsulation of concentrated hemoglobin solution in phospholipid vesicles retards the reaction with NO, but not CO, by intracellular diffusion barrier. *J Biol Chem* 283: 1508–1517, 2008.
22. **Sakai H, Sato A, Takeoka S, Tsuchida E.** Rheological properties of hemoglobin vesicles (artificial oxygen carriers) suspended in a series of plasma-substitute solutions. *Langmuir* 23: 8121–8128, 2007.
23. **Sakai H, Sou K, Horinouchi H, Kobayashi K, Tsuchida E.** Haemoglobin-vesicles as artificial oxygen carriers: present situation and future visions. *J Intern Med* 263: 4–15, 2008.
24. **Sakai H, Suzuki Y, Kinoshita M, Takeoka S, Maeda N, Tsuchida E.** O_2 release from Hb vesicles evaluated using an artificial, narrow O_2-permeable tube: comparison with RBCs and acellular Hbs. *Am J Physiol Heart Circ Physiol* 285: H2543–H2551, 2003.
25. **Sakai H, Tsai AG, Kerger H, Park SI, Takeoka S, Nishide H, Tsuchida E, Intaglietta M.** Subcutaneous microvascular responses to hemodilution with a red cell substitute consisting of polyethyleneglycol-modified vesicles encapsulating hemoglobin. *J Biomed Mater Res* 40: 66–78, 1998.
26. **Schmid-Schönbein H, Wells R.** Fluid drop like transition of erythrocytes under shear. *Science* 165: 288–291, 1969.
27. **Secomb TW, Hsu R, Pries AR.** Motion of red blood cells in a capillary with an endothelial surface layer: effect of flow velocity. *Am J Physiol Heart Circ Physiol* 281: H629–H636, 2001.
28. **Shevkoplyas SS, Yoshida T, Gifford SC, Bitensky MW.** Direct measurement of the impact of impaired erythrocyte deformability on microvascular network perfusion in a microfluidic device. *Lab Chip* 6: 914–920, 2006.
29. **Skalak R, Branemark PI.** Deformation of red blood cells in capillaries. *Science* 164: 717–719, 1969.
30. **Skalak R, Tozeren H.** Flow mechanics in the microcirculation. In: *Mathematics of Microcirculation Phenomena*, edited by Gross JF and Popel A. New York, NY: Raven, 1980, p. 17–40.
31. **Tateishi N, Suzuki Y, Cicha I, Maeda N.** O_2 release from erythrocytes flowing in a narrow O_2-permeable tube: effects of erythrocyte aggregation. *Am J Physiol Heart Circ Physiol* 281: H448–H456, 2001.
32. **Thorsen T, Maerkl SJ, Quake SR.** Microfluidic large-scale integration. *Science* 298: 580–584, 2002.
33. **Tilles AW, Eckstein EC.** The near-wall excess of platelet-sized particles in blood flow: its dependence on hematocrit and wall shear rate. *Microvasc Res* 33: 211–223, 1987.
34. **Whitmore RL.** *Rheology of the Circulation*. Oxford, UK: Pergamon, 1968.
35. **Zhang J, Johnson PC, Popel AS.** An immersed boundarylattice Boltzmann approach to simulate deformable liquid capsules and is application to microscopic blood flows. *Phys Biol* 4: 285–295, 2007.

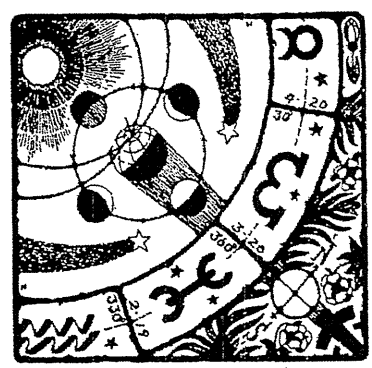

Mechanism of Flocculate Formation of Highly Concentrated Phospholipid Vesicles Suspended in a Series of Water-Soluble Biopolymers

Hiromi Sakai,*,† Atsushi Sato,‡,§ Shinji Takeoka,|| and Eishun Tsuchida*,†

Research Institute for Science and Engineering, Graduate School of Advanced Science and Engineering, and Consolidated Research Institute for Advanced Science and Medical Care, Waseda University, Tokyo 169-8555, Japan

Received April 21, 2009; Revised Manuscript Received May 23, 2009

Polyethylene glycol-modified vesicles (liposomes) encapsulating hemoglobin (HbV) are artificial oxygen carriers that have been developed as a transfusion alternative. The HbV suspension in an albumin solution is nearly Newtonian; other biopolymers, hydroxyethyl starch (HES), dextran (DEX), and modified fluid gelatin, induce flocculation of HbVs through depletion interaction and render the suspensions as non-Newtonian. The flocculation level increased with hydrodynamic radius (R_h) or radius of gyration (R_g) of series of HES or DEX with different molecular weights at a constant polymer concentration (4 wt %). However, the flocculation level differed markedly among the polymers. A crowding index (C_i) representing the crowding level of a polymer solution is defined as (excluded volume of one polymer) × (molar concentration) × Avogadro's number, using R_h or R_g. All polymers' flocculation level increases when C_i approaches 1: when the theoretical total excluded volumes approach the entire solution volume, the excluded HbV particles are forced to flocculate.

Introduction

Hemoglobin vesicles (HbVs) are artificial oxygen carriers that encapsulate a concentrated Hb solution in phospholipid vesicles (liposomes, 280 nm particle diameter).[1,2] In contrast to conventional liposomal products, the HbV suspension concentration must be extremely high (Hb, 10 g/dL; lipids, 5−6 g/dL). One injection as a transfusion alternative causes the substitution of a large volume of blood, for example, 40% of the circulating blood volume.[3,4] Accordingly, it is important to evaluate the suspension rheology of HbV, which might influence hemorheology after intravenous administration.[5]

Albumin, dissolved in a blood plasma at 4−5 wt %, provides sufficient colloid osmotic pressure (COP, 13−20 Torr) to play an important role in equilibrating COP between blood and interstitial fluid, thereby maintaining the overall blood volume. This COP is one requisite for a transfusion alternative to sustain blood circulation for transporting oxygen and metabolites. One HbV contains about 30000 Hb molecules. Therefore, an HbV suspension shows no COP in an aqueous solution. Accordingly, HbVs must be suspended in, or coinjected with, a plasma substitute solution. Animal tests of HbVs suspended in plasma-derived human serum albumin (HSA) or recombinant HSA (rHSA) exhibited oxygen transporting capacity that is comparable to that of blood.[3,4,6,7] We reported previously that HbVs suspended in plasma-derived HSA or rHSA were almost Newtonian and that no aggregation was detected microscopically.[8,9] On the other hand, various plasma substitutes are used worldwide, such as hydroxyethyl starch (HES), dextran (DEX), and modified fluid gelatin (MFG).[10,11] These water-soluble biopolymers have been shown to induce flocculate formation of HbVs and to render the suspensions non-Newtonian.[5,12] A larger HES tended to induce stronger flocculate formation.[13]

Generally, water-soluble polymers interact with particles such as polystyrene beads, silica, liposomes, and red blood cells (RBCs) to induce aggregation or flocculation.[5,14−21] So-called "macromolecular crowding" by water-soluble polymers is known to induce precipitation or unfolding of proteins and DNA and modify their functions.[22,23] However, the mechanism of liposomal flocculation induced using a polymer has remained controversial.

As described herein, we sought a universal explanation of flocculate formation for PEG-modified vesicles suspended in a series of plasma substitutes and related biopolymers with different molecular weights. We used common methods in the field of polymer science, viscometry and membrane osmometry of polymer solutions, to estimate the size and the excluded volume effect of the biopolymers that are believed to be nonadsorbing to the surface of PEG-modified vesicles, even in a highly concentrated suspension.

Materials and Methods

Preparation of HbVs. The HbVs used for this study were prepared under sterile conditions, as reported previously.[24−27] The Hb was purified from outdated donated blood provided by the Japanese Red Cross Society (Tokyo, Japan). The encapsulated purified Hb (38 g/dL) contained 14.7 mM of pyridoxal 5′-phosphate (PLP; Sigma-Aldrich Corp.) as an allosteric effector at a molar ratio of PLP/Hb = 2.5. The lipid bilayer comprised a mixture of 1,2-dipalmitoyl-*sn*-glycero-3-phosphatidylcholine, cholesterol, and 1,5-bis-*O*-hexadecyl-*N*-succinyl-L-glutamate (DHSG) at a molar ratio of 5/5/1 (Nippon Fine Chemical Co. Ltd., Osaka, Japan) and 1,2-distearoyl-*sn*-glycero-3-phosphatidylethanolamine-*N*-poly(ethylene glycol) (NOF Corp., Tokyo, Japan, 0.3 mol % of the total lipid). The particle diameter was 279 ± 95 nm. The HbVs were suspended in a physiologic saline solution at [Hb] = 10

* To whom correspondence should be addressed. Tel.: +81-3-5286-3120. Fax: +81-3-3205-4740. E-mail: hiromi@waseda.jp (H.S.); eishun@waseda.jp (E.T.).
† Research Institute for Science and Engineering.
‡ Graduate School of Advanced Science and Engineering.
§ Present affiliation: NOF Corporation, Tokyo, Japan.
|| Consolidated Research Institute for Advanced Science and Medical Care.

10.1021/bm900455e CCC: $40.75
Published on Web 07/02/2009

Table 1. Molecular Weights and Colloid Osmotic Pressures (COP) of Plasma Substitute Solutions at 4 wt %[a]

plasma substitute solutions	M_w (kDa)	M_n (kDa)	M_w/M_n	COP (Torr)
DEX_{40}	42[b]	22[b]	1.9	29
DEX_{70}	73[b]	38[b]	1.9	25
DEX_{200}	184[b]	84[b]	2.2	18
DEX_{500}	505[b]	737[c]		14
HES_{70}	68[b]	17[b]	4.0	21
HES_{130}	130[b]	50[b]	2.6	21
HES_{200}	240[b]	70[b]	3.4	15
HES_{670}	670[b]	194[c]	3.5	13
MFG	30[b]	23[b]	1.3	44
rHSA	67[b]	67[b]	1.0	13

[a] DEX, dextran; HES, hydroxyethyl starch; MFG, modified fluid gelatin; rHSA, recombinant human serum albumin. [b] Data provided by the manufacturer. [c] Calculated from the concentration dependence of COP (unpublished data).

g/dL ([lipids] = 6 g/dL). Then they were deoxygenated for storage with N_2 bubbling in vials.[28]

Water-Soluble Biopolymers. The plasma substitutes and water-soluble biopolymers used for this study are listed in Table 1. An MFG solution (Gelofusin, M_w 30 kDa, 4 wt % in a physiological saline solution) was a gift from B. Braun Melsungen AG (Melsungen, Germany). The concentration of MFG, 4 wt %, is the lowest among those of the commercially available plasma substitute solutions. Therefore, we fixed this concentration for all polymer solutions in this experiment. Recombinant human serum albumin (rHSA, M_w 67 kDa, 25 wt %) was a gift from Nipro Corp. (Osaka, Japan). Before use, it was diluted to 4-wt% using saline solution (Otsuka Pharmaceutical Co. Ltd., Osaka, Japan). Powdered DEX_{40}, DEX_{70}, DEX_{200}, and DEX_{500} (M_w 40, 70, 200, and 500 kDa, respectively; Sigma-Aldrich Corp.) were dissolved in saline solution at the concentration of 4 wt %. An HES_{70} solution (Saline-HES, M_w 70 kDa, 6 wt % in a physiological saline solution) was purchased from Kyorin Pharmaceutical Co. Ltd. (Osaka, Japan). An HES_{130} solution (Voluven, M_w 130 kDa, 6 wt % in a physiological saline solution) and powdered HES_{200} (HES200/0.5, M_w 200 kDa) were gifts from Fresenius Kabi AG (Homburg v.d.H., Germany). The HES_{70} and HES_{130} solutions were diluted to 4 wt %. The HES_{200} was dissolved in a physiological saline solution at 4 wt %. An HES_{670} solution (Hextend, M_w 670 kDa, 6 wt % in a physiological Ringer lactate solution) was obtained from Hospira Inc. (Lake Forest, IL) and diluted to 4 wt %.

Preparation of HbVs Suspended in Plasma Substitutes. The HbVs suspended in a saline solution were ultracentrifuged (20000 × *g*, 30 min) to produce HbV-particle sediment. After removal of the upper saline solution, a polymer solution (4 wt %) was added and the HbVs were redispersed by stirring and vortexing; the final concentration was adjusted to [Hb] = 10 g/dL. Immediately before viscometric measurement, the suspension was filtrated (0.45 μm pore size, Dismic; Toyo Roshi Kaisha Ltd., Tokyo, Japan). For visualization of the HbV flocculation formation, HbVs suspended in DEX_{500} and rHSA were diluted 20 times with the corresponding polymer solutions and observed using a microscope (IX-71, Olympus Corp., Tokyo).

Colloid Osmotic Pressure (COP) Measurement of Polymer Solutions To Obtain Radius of Gyration. The COP of the polymer solution was measured using a membrane osmometer (Model 4420; Wescor Inc., Logan, USA, Membrane cutoff M_w = 10000).[29] The polymer solutions were diluted with saline, with COP values obtained at each concentration. The COP data were analyzed using thermodynamic equations for reduction in the chemical potential of the solvent caused by the presence of a solute.[30] The relation with the COP (Π) and the polymer concentration (*C*) is given as eq 1.

$$\Pi/C = R \cdot T/M_n + R \cdot T \cdot B \cdot C \quad (1)$$

In that equation, *R* is the gas constant, *T* represents the temperature in degrees Kelvin (K), M_n is the number averaged molecular weight, and *B* is the second virial coefficient. The latter provides a measure of solution ideality. The M_n of each polymer solution is determined from the intercept obtained from linear least-squares regression of plots Π/*C* versus *C*. The value of *B* is obtained from the slope.

The obtained M_n and *B* were inserted into eq 2 to calculate the radius of gyration (R_g)

$$R_g = \left(\frac{3[M_n]^2 B}{16\pi N}\right)^{1/3} \quad (2)$$

where *N* is Avogadro's number.

Viscosity Measurement of Polymer Solutions To Obtain the Hydrodynamic Radius. Steady-shear viscosity measurements were performed using a rheometer (Physica MCR 301; Anton Paar GmbH, Graz, Austria).[5] The cone diameter was 50 mm; the gap angle between the cone and plate was 1°. All measurements were performed at 25 °C. About 650 μL of the sample was sandwiched between the cone and plate. The excess solution was wiped out.

The hydrodynamic radius, R_h, for each plasma substitute solution was obtained using the viscosity measurement and the following equations.[31] The intrinsic viscosity of each plasma substitute solution [η] was obtained by measuring the concentration dependence of the viscosity, η, at 1000 s^{-1} and from eqs 3 and 4.

$$[\eta] = \lim_{C \to 0}(\eta_{sp}/C) \quad (3)$$

$$\eta_{sp} = (\eta - \eta_0)/\eta_0 \quad (4)$$

Therein, η_0 is the solvent viscosity and η_{sp} is the specific viscosity of the polymer solution. According to the Einstein viscosity relation, eq 5, [η] is expressed as eq 6.

$$\eta = \eta_0(1 + 2.5\phi) \quad (5)$$

$$[\eta] = (2.5 \cdot N \cdot V_e)/M \quad (6)$$

In those equations, V_e is the volume of an equivalent spherical particle; it is expressed as eq 7.

$$V_e = (4\pi \cdot R_h^3)/3 \quad (7)$$

From eqs 6 and 7, the hydrodynamic radius R_h is expressed as eq 8.[31]

$$R_h = \left(\frac{3[\eta]M}{10\pi N}\right)^{1/3} \quad (8)$$

Viscosity Measurement of HbVs Suspended in Plasma Substitute Solutions. The viscosity of the HbVs suspended in each plasma substitute solution was measured using the same method as that described above. The shear rate was decreased from 10^3 to 10^{-4} s^{-1}. Most of the HbV suspensions are non-Newtonian fluids. They show shear thinning profiles because of the presence of flocculation. Flocculation dissociates at a higher shear rate. We defined the flocculation index (F_i) using eq 9.

$$F_i = (\eta_{10} - \eta_0)/(\eta_{1000} - \eta_0) \quad (9)$$

In that equation, η_{10} and η_{1000}, respectively, represent the viscosity at the shear rates of 10 and 1000 s^{-1}. The excluded volume V_{ex} of one hydrated polymer sphere is four times larger than its V_e (the volume of

an equivalent spherical particle).[32] Therefore, the excluded volume is expressed as eq 10.

$$V_{ex} = 4 \cdot V_c = 4 \cdot (4\pi R^3/3), \quad R = R_h \text{ or } R_g \tag{10}$$

A crowding index (C_i), a parameter to express the level of crowding by polymer chains in a polymer solution, was defined as shown in eq 11.

$$C_i = V_{ex} \cdot C \cdot N \tag{11}$$

Therein, N is Avogadro's number and C is the molar concentration of the polymer converted from 4 wt %. To elucidate the flocculation mechanism, F_i is shown against R_h, R_g, ${}^{\Pi}V_{ex}$, ${}^{\eta}V_{ex}$, ${}^{\Pi}C_i$, and ${}^{\eta}C_i$. For these symbols, superscripts Π and η signify that the parameters are derived, respectively, from COP and viscosity measurement of polymer solutions.

Estimation of Depletion Energy. Asakura and Oosawa, who first described the depletion flocculation mechanism,[33] calculated the interaction energy through geometrical analyses of particles and polymers. Our analyses assume that two spherical particles, HbVs, with radius a (=140 nm) are dispersed in a solution of rigid spherical polymer coils, plasma substitutes. The depletion-free attraction E_{dep} at surface separation d of less than twice R_g is given as eq 12.[34,35]

$$-E_{dep} = (\pi \cdot N_p/12) \cdot (2R_g - d)^2 \cdot (6a + 4R_g + d) \cdot k \cdot T \tag{12}$$

In that equation, N_p is the number density of polymer molecules, k is the Boltzmann's constant, and T is the absolute temperature (=298 K). The surface separation distance d was assumed to be 1, 2, 3, 4, 5, and 6 nm; F_i is shown against $-E_{dep}$ for all polymers.

Results

R_g, R_h, V_{ex}, and C_i of the Polymer Solutions Calculated from Π and η. The COPs of polymer solutions (Π) were measured at different concentrations (C) and Π/C was plotted versus C (Figure 1A). All polymers exhibited linear relations. The least-squares approach was used. The R_g values obtained from eq 2 are presented in Table 2.

Figure 1B shows viscosities of polymer solutions measured at different concentrations. The plots of η_{sp}/C versus C are shown. All polymer solutions showed linear relations. After least-squares regression was performed, R_h values were obtained from $[\eta]$ and eq 8; they are presented in Table 2.

Values of ${}^{\Pi}V_{ex}$, ${}^{\eta}V_{ex}$, ${}^{\Pi}C_i$, and ${}^{\eta}C_i$ were calculated using eqs 10 and 11 with R_h or R_g at a polymer concentration of 4 wt %. The values are presented in Table 2. Both DEX and HES showed larger R_h or R_g with increasing molecular weights.

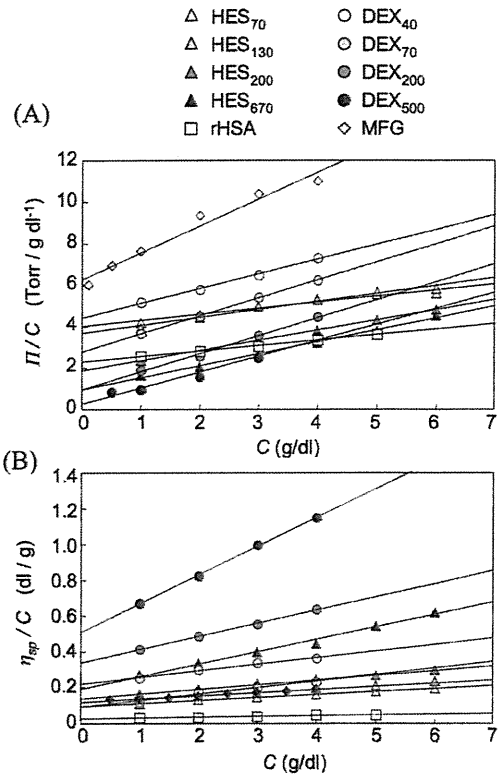

Figure 1. (A) Colloid osmotic pressure data shown as Π/C versus C, where Π is the colloid osmotic pressure (Torr) and C is the polymer concentration (g/dL). (B) Viscosity data of polymer solutions are shown as η_{sp}/C versus C, where η_{sp} is the specific viscosity (−) and C is the polymer concentration (g/cm^3).

Consequently, V_{ex} and C_i also increased. Actually, rHSA showed the lowest C_i.

Rheological Properties of HbVs Suspended in a Series of Polymer Solutions and F_i. Figure 2 portrays the viscosity of HbVs suspended in various plasma substitute solutions when the shear rate was decreased from 10^3 to 10^{-4} s^{-1}. The HbVs suspended in rHSA constituted a nearly Newtonian fluid and showed the lowest viscosity. Because of the detection limit of shear strain of this rheometer and the very low viscosity of HbV-rHSA, only measurements greater than 7×10^{-1} s^{-1} were valid. On the other hand, HbVs suspended in other polymer solutions, HES, DEX, and MFG, exhibited non-Newtonian properties with a high viscosity at lower shear rates, so-called "shear-thinning", attributable to the flocculate formation of HbVs. The viscosities were measurable in a wider range of shear rates.

Using the viscosity data, the flocculation index, presented in Table 3, was calculated using eq 9. It is apparent that F_i

Table 2. Plasma Substitute Solutions and Their Physicochemical Properties at 4 wt %

		parameters obtained by Π			parameters obtained by η		
plasma substitute solutions	C (mM)	R_g (nm)	${}^{\Pi}V_{ex}$ (nm^3)	${}^{\Pi}C_i$	R_h (nm)	${}^{\eta}V_{ex}$ (nm^3)	${}^{\eta}C_i$
DEX_{40}	0.957	4.1	1154	0.667	3.94	1025	0.591
DEX_{70}	0.550	5.9	3441	1.141	6.34	4270	1.416
DEX_{200}	0.217	12	28952	3.784	9.97	16605	2.170
DEX_{500}	0.079	28.2	375747	17.92	15.98	68372	3.261
HES_{70}	0.588	3.2	549	0.194	4.68	1717	0.608
HES_{130}	0.308	3.8	919	0.170	6.13	3859	0.715
HES_{200}	0.167	6.4	4392	0.441	8.08	8838	0.887
HES_{670}	0.060	10.5	19396	0.697	12.68	34159	1.228
MFG	1.333	3.9	994	0.798	3.83	941	0.756
rHSA	0.602	4.5	1527	0.553	3.08	490	0.177

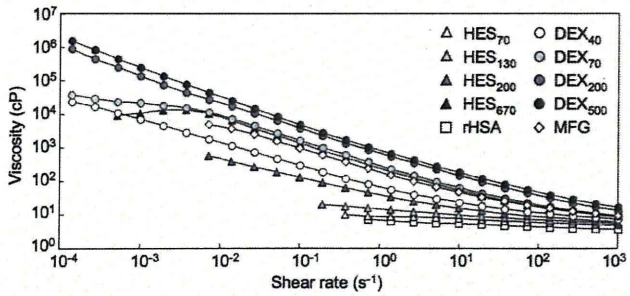

Figure 2. Viscosity of HbVs suspended in various water-soluble biopolymers. [Hb] = 10 g/dL, 25 °C.

Table 3. Viscosities of HbVs Suspended in Polymer Solutions (4 wt %) and Flocculation Index (F_i). [Hb] = 10 g/dL

polymer solution for HbV suspension	viscosity (cP) at 10 s^{-1}	viscosity (cP) at 1000 s^{-1}	F_i
DEX_{40}	23.1	7.5	3.78
DEX_{70}	64.3	9.3	8.84
DEX_{200}	146	13.3	14.22
DEX_{500}	181.5	16.8	15.29
HES_{70}	7.7	4.9	1.88
HES_{130}	9.7	5.5	2.10
HES_{200}	15.6	6.1	3.21
HES_{670}	53.0	8.9	8.05
MFG	46.7	9.3	5.91
rHSA	5.3	3.6	1.68

increased concomitantly with increasing molecular weights of both HES and DEX.

Figure 3 is the microscopic view of the flocculate formation of HbV when suspended in DEX_{500}; the combination showing the highest F_i. Numerous indeterminate forms of flocculation were apparent. On the other hand, HbV suspended in rHSA were dispersed homogeneously (data not shown here). No flocculation was detected.

Relation between F_i and Physicochemical Properties of Polymer Solutions. In Figure 4A, the flocculation index F_i is shown against R_g and R_h. The tendency of increase in F_i with R_g and R_h is apparent. However, the polymers show some differences. In Figure 4B, F_i is shown against the excluded volume of polymers ($^{\Pi}V_{ex}$ and $^{\eta}V_{ex}$ obtained, respectively, from R_g and R_h, using eq 10). The differences are magnified in comparison with Figure 4A. In Figure 4C, F_i is shown against the crowding indexes $^{\Pi}C_i$ and $^{\eta}C_i$ of all polymers; the plots tended to create single sigmoidal curves. Actually, F_i starts to increase when $^{\Pi}C_i$ and $^{\eta}C_i$ are greater than 0.6. The steepest curves are at around 1, where the sum of the excluded volumes of the polymer molecules becomes greater than the entire volume of the solution.

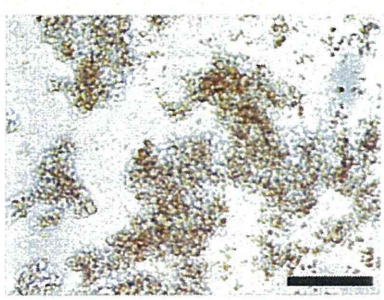

Figure 3. Microscopic view of the flocculates of HbV when suspended in DEX_{500}. The scale bar is 100 μm.

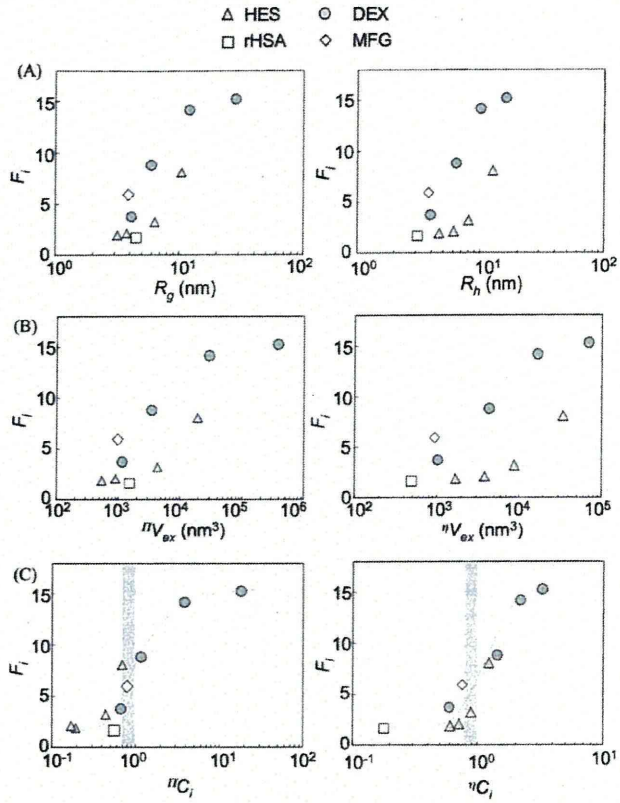

Figure 4. Flocculation index (F_i) values of HbVs suspended in water-soluble polymers are shown against (A) polymer sizes R_g and R_h, (B) excluded volumes of one polymer chain, $^{\Pi}V_{ex}$ and $^{\eta}V_{ex}$, and (C) the crowding index of the polymer solution, $^{\Pi}C_i$ and $^{\eta}C_i$.

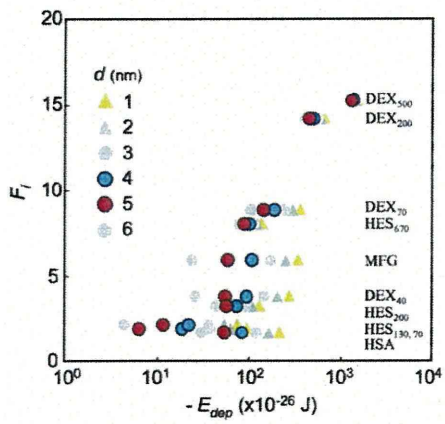

Figure 5. Flocculation index (F_i) of HbVs suspended in water-soluble polymers is shown against depletion energies ($-E_{dep}$) calculated assuming that the surface distance, d, of flocculated HbVs is 1−6.

Estimation of Depletion Energy. Depletion energy E_{dep} was estimated using eq 12. No data are available for surface separation distance d. We calculated E_{dep} in cases of $d = 1-6$ because $d < 2R_g$, and the smallest $2R_g$ is 6.4 for HES_{70}. As portrayed in Figure 5, a suspension of the higher flocculation index shows higher ($-E_{dep}$) for all d values. Actually, $-E_{dep}$ for HbVs suspended in DEX_{500} showed the largest value of 1.3 $\times$ 10^{-23} J. When d is 1−3 nm, HES_{670} showed smaller $-E_{dep}$ than that of either MFG or DEX_{40}, in spite of a larger F_i for HES_{670}. When d is 6 nm, HES_{200} showed larger $-E_{dep}$ than that of either MFG and DEX_{40}, in spite of a smaller F_i for HES_{200}. No such discrepancy is apparent and a critical $-E_{dep}$ is the most

evident when d is 4 or 5 nm. It is estimated that the surface separation distance of the HbV flocculation would be 4−5 nm.

Discussion

Our primary finding is that the flocculate formation of phospholipid vesicles (liposomes) suspended in water-soluble biopolymers of various kinds is explained simply by the crowding index, even though the structures and physicochemical characteristics of the polymers differ.

Both DEX and HES are polysaccharides. The DEX chain consists of α-1,6 glycosidic linkages between glucose molecules, although branches begin from α-1,4 linkages (and in some cases, α-1,2 and α-1,3 linkages as well). In contrast, HES is made from starch, a rather linear polysaccharide of glucose linked mainly by α-1,4 linkages that promote the formation of a helix structure. Starch is easily hydrolyzed by amylase in blood. The hydroxyl groups of the polysaccharide backbone are substituted with hydroxyethyl group to prevent such degradation. The degree of substitution (DS) differs among the various HES solutions of the companies. A major plasma protein, HSA, has a globular structure and negative charges (pI = 4.8) at a physiological condition. Finally, MFG is made of hydrolyzed gelatin, which is then cross-linked randomly with succinic acid; it is also a negatively charged polymer. In spite of such complexity to compare the structures of these polymers, an important matter related to expression of flocculation is the extent to which the polymer solution is crowded with the polymer chains, that is, crowding index C_i.

Liposomes are well-known to form flocculates or aggregates in the presence of water-soluble polymers that were analyzed mainly by turbidity or light-scattering measurements at a very low concentration,[14,15,36] where a suspension would consist of a collection of discrete flocculates. On the other hand, the present HbV suspension consists of highly concentrated HbV with the weight fraction of nearly 16 g/dL in all and a volume fraction of about 40 vol %. For such particle dispersion, we used a rheometer to measure the flocculate formation of HbVs directly.[5,12,37] The HbVs suspended in rHSA constituted a nearly Newtonian fluid. In contrast, HbVs suspended in other polymer solutions, HES, DEX, and MFG, showed non-Newtonian properties with a high viscosity at a lower shear rate (shear-thinning) because of the flocculation of HbVs. A series of HES and DEX solutions showed a clear molecular-weight dependence to induce flocculation. For all combinations of HbVs and a polymer solution, the flocculation of HbVs dissociates at a higher shear rate and the flocculation-dissociation reaction is completely reversible.[5]

The mechanism of liposome flocculation has remained controversial. A plausible and classical idea is that polymer chains (DEX or PEG) adsorb directly on the surface of the particles to produce bridges.[15,36] The data presented herein might show simply that a larger polymer would induce more numerous adsorption points and stronger bridges. Nevertheless, a PEG aqueous solution and a polysaccharide aqueous solution are well-known to be immiscible; that fails to explain the adsorption of DEX and HES on the surface of PEG-modified HbVs. Actually, Kawakami et al.[38] clarified that interactions between the liposomal surface without PEG modification and water-soluble polymers are very small and that DEX does not adsorb onto the surface of liposomes. Another mechanism was that (i) hydration of polymer chains would deprive water molecules from particles and thereby exclude the particles from the bulk solution.[17] However, this was contradicted by Meyuhas et al.[14] because of the fact that dialysis of liposomes against polymer-containing solutions did not induce flocculation, although direct addition of the polymer to the liposomes solution induced flocculation. Recent practical and theoretical analyses contradict these theories and suggest a depletion mechanism: (ii) A depletion layer develops near a particle surface that is in contact with a polymer solution if the loss of the configurational entropy of the coil of the polymer is not balanced by adsorption energy.[35,39,40] Within this layer, the polymer concentration is lower than in the bulk phase. Consequently, as particles approach, the osmotic pressure difference between the interparticle polymer-poor depletion layer and the bulk phase engenders solvent displacement into the bulk phase and consequent depletion interaction. Because of this interaction, the attractive force of particles tends to minimize the polymer-poor space between the particles, thereby inducing flocculation.[14,18,41−43] In this case, the polymer coil size in comparison to the interparticle spacing is important. Results of our previous study demonstrated that the viscosity and G' of our flocculated HbV dispersions are considerably lower than those of other particle dispersions of irreversible aggregation induced by polymer adsorption onto the particles,[35] indicating that the interparticle interaction would be considerably less in our system and that depletion interaction is plausible.

We obtained the radii of polymers as R_g and R_h using different methods: R_h is the hydrodynamic radius of a polymer coil in a flow condition; R_g is the radius of gyration obtained using the second virial coefficient, which provides a measure of solution ideality. The meanings of these parameters differ. Actually, we were unable to obtain identical values for each polymer. However, a tendency exists by which a polymer with a higher molecular weight shows larger R_g or R_h. Using these parameters, we calculated the excluded volume of each polymer as ${}^{\Pi}V_{ex}$ and ${}^{\eta}V_{ex}$. In contrast to the clear relation between R_h and the level of RBC flocculation reported by Armstrong et al.,[31] our data (Figure 4A and B) demonstrate that the size of one polymer chain is insufficient to explain the level of flocculation of HbVs because the polymer species dependencies are evident.

As described in this paper, we defined the crowding index C_i, which includes not only the parameters of size and extended volume but also the concentration of the polymer solution. The value of C_i is calculated from R_g and R_h of an extremely diluted polymer solution ($C \to 0$), where the polymer is highly extended. A polymer solution with a higher molecular weight exceeds $C_i = 1$, indicating that the polymer cannot be highly extended and that the solution is congested with polymer chains. The volume of extended polymer chains occupies the entire volume of the solution, which would strengthen the exclusion effect. This situation would enhance the exclusion effect from the hydrated sphere of the vesicles, creating a more flocculated structure of the vesicles. The plots of F_i versus C_i of different polymers created a single sigmoidal curve, showing that whether C_i of a polymer solution is greater or less than 1 is one indicator to determine the flocculate formation of phospholipid vesicles (liposomes).

Using eq 12, we estimated the depletion energy of all suspensions. A clear critical E_{dep} is obtained when the interparticle distance in the HbV flocculation is 4−5 nm (Figure 5). This interparticle distance is slightly less than the sizes of the polymers, rHSA, HES_{70}, and HES_{130}, which do not induce flocculation remarkably. The larger polymers induce flocculation in the following order: $HES_{200} < DEX_{40} < MFG < HES_{670} < DEX_{70} < DEX_{200} < DEX_{500}$. The interparticle distance of 4−5 nm would no longer enable these larger polymers to enter into

the interparticle space. However, it must be emphasized that eq 12 incorporates not only the relation between the sizes, but also the polymer concentrations for COP, which differ among polymer solutions.

The critical E_{dep} to induce flocculation was calculated as shown in Figure 5. The meaning of this value is difficult to interpret. In contrast, the concept of C_i simplifies estimation of the level of flocculate formation for the selected polymers because it is reasonable to imagine that the particles would be forced to be flocculated and the phase separated when the extended polymer chains occupy the entire volume of the solution ($C_i = 1$).

One might wonder whether a blood plasma would induce flocculation. To estimate C_i of plasma proteins, we selected common and gigantic proteins: fibrinogen (M_w = 340 kDa, concentration < 0.4 wt %, R_h = 10.95 nm[31]), IgA (162 kDa, <0.41 wt %, 6.5 nm[31]), IgG (150 kDa, <1.7 wt %, 5.29 nm[31]), IgM (950 kDa, <0.26 wt %, 12.65 nm[31]), and albumin (67 kDa, 4 wt %, 3.08 nm). The sum of C_i of the whole plasma is calculated as around 0.626. This is plausible because we have already reported that PEG-modified HbV shows no flocculation in blood.[8,9]

The concentration of plasma substitutes used in the flocculate experiment (4 wt %) is higher than that in plasma when they are clinically infused (i.e., 0.5−1 wt %) because they are diluted with blood. In such a condition, flocculation of PEG-modified HbV would not occur because C_i becomes less than 1, as shown by the curves presented in Figure 4C. However, only DEX_{500} would show $^{II}C_i$ higher than 1 and $^{\eta}C_i$ nearly 1. This explains well that the intravenous administration of DEX_{500} facilitates RBC aggregation, as reported by Bishop et al.,[20] even after dilution with blood.

An important limitation of our study is that we selected water-soluble polymers that are used clinically as plasma expanders (HSA, MFG, HES, and DEX), and selected DEX with different molecular weights. Other water-soluble polymers, cationic, anionic, or otherwise, would show different rheological properties. Actually, HbV contains a negatively charged lipid (DHSG). For that reason, the HbV surface is negatively charged.[44] However, this is shielded by the extended PEG chains and the presence of NaCl. The dissociation level of the carboxylic acid group depends on pH. In pure water, the zeta potential is magnified and tends to prevent flocculation of vesicles. Additional study is necessary when liposomes are used for purposes other than as blood substitutes.

Our data show that the rheological property of phospholipid vesicles suspension is adjustable by the combination of water-soluble biopolymers by inducing flocculate formation and hyperviscosity.[5] Reports show that hyperviscosity would not necessarily be deteriorative and might, in some cases, be advantageous in the body.[45] A higher plasma viscosity causes a higher shear stress on the vascular wall, inducing vasorelaxation and improved microcirculation.[46−48] The combination of HbV and water-soluble polymers provides a unique opportunity to manipulate the suspension rheology for use in various applications.[49,50]

Conclusion

In this study, we defined a crowding index (C_i) representing the crowding level of a biopolymer solution. Results clarified that the level of flocculation of phospholipid vesicles increases uniformly for all biopolymers when C_i approaches 1. In this situation, the theoretical total excluded volume approaches and exceeds the entire volume of the solution. This simplified explanation is useful to understand flocculation and aggregation of particles, including liposomes and red blood cells, in various situations.

Acknowledgment. The authors acknowledge Dr. Masuhiko Takaori (Higashi Takarazuka Satoh Hospital). The rHSA, HES, and MFG used for this study were, respectively, gifts from Nipro Corp., Fresenius Kabi A.G., and B. Braun. This study was supported by Health and Labour Sciences Research Grants (Research on Regulatory Science of Pharmaceuticals and Medical Devices), Ministry of Health, Labour and Welfare, Japan (H.S., E.T.), and a Grant-in-Aid for Scientific Research from the Japan Society for the Promotion of Science (B16300162; H.S.).

References and Notes

(1) Sakai, H.; Sou, K.; Horinouchi, H.; Kobayashi, K.; Tsuchida, E. *J. Intern. Med.* **2008**, *263*, 4–15.
(2) Tsuchida, E.; Sou, K.; Nakagawa, A.; Sakai, H.; Komatsu, T.; Kobayashi, K. *Bioconjugate Chem.* [Online early access]. DOI: 10.1021/bc800431d. Published Online: Feb 10, 2009. http://pubs.acs.org/doi/full/10.1021/bc800431d.
(3) Sakai, H.; Horinouchi, H.; Yamamoto, M.; Ikeda, E.; Takeoka, S.; Takaori, M.; Tsuchida, E.; Kobayashi, K. *Transfusion* **2006**, *46*, 339–347.
(4) Sakai, H.; Masada, Y.; Horinouchi, H.; Yamamoto, M.; Ikeda, E.; Takeoka, S.; Kobayashi, K.; Tsuchida, E. *Crit. Care Med.* **2004**, *32*, 539–545.
(5) Sakai, H.; Sato, A.; Takeoka, S.; Tsuchida, E. *Langmuir* **2007**, *23*, 8121–8128.
(6) Izumi, Y.; Sakai, H.; Hamada, K.; Takeoka, S.; Yamahata, T.; Kato, R.; Nishide, H.; Tsuchida, E.; Kobayashi, K. *Crit. Care Med.* **1996**, *24*, 1869–1873.
(7) Yamazaki, M.; Aeba, R.; Yozu, R.; Kobayashi, K. *Circulation* **2006**, *114*, I220–I225.
(8) Sakai, H.; Takeoka, S.; Park, S. I.; Kose, T.; Nishide, H.; Izumi, Y.; Yoshizu, A.; Kobayashi, K.; Tsuchida, E. *Bioconjugate Chem.* **1997**, *8*, 23–30.
(9) Sakai, H.; Tsai, A. G.; Kerger, H.; Park, S. I.; Takeoka, S.; Nishide, H.; Tsuchida, E.; Intaglietta, M. *J. Biomed. Mater. Res.* **1998**, *40*, 66–78.
(10) Webb, A. R.; Nash, G. B.; Dormandy, J. A.; Bennett, E. D. *Clin. Hemorheol.* **1990**, *10*, 287–296.
(11) Tatara, T.; Tashiro, C. *Biomacromolecules* **2005**, *6*, 1732–1738.
(12) Sato, A.; Sakai, H.; Takeoka, S.; Tsuchida, E. *Hemorheol. Related Res. (Nippon Hemorheol. Gakkai-shi)* **2007**, *10*, 3–11 (in Japanese).
(13) Sato, T.; Sakai, H.; Sou, K.; Medebech, M.; Glatter, O.; Tsuchida, E. *J. Phys. Chem. B* **2009**, *113*, 8418−8428.
(14) Meyuhas, D.; Nir, S.; Lichtenberg, D. *Biophys. J.* **1996**, *71*, 2602–2612.
(15) Sunamoto, J.; Iwamoto, K.; Kondo, H. *Biochem. Biophys. Res. Commun.* **1980**, *94*, 1367–1373.
(16) Otsubo, Y. *Langmuir* **1990**, *6*, 114–118.
(17) Tilcock, C. P.; Fisher, D. *Biochim. Biophys. Acta* **1982**, *688*, 645–652.
(18) Neu, B.; Meiselman, H. J. *Biophys. J.* **2002**, *83*, 2482–2490.
(19) Goto, Y.; Sakakura, S.; Hatta, M.; Sugiura, Y.; Kato, T. *Acta Anaesthesiol. Scand.* **1985**, *29*, 217–223.
(20) Bishop, J. J.; Nance, P. R.; Popel, A. S.; Intaglietta, M.; Johnson, P. C. *Am. J. Physiol. Heart Circ. Physiol.* **2001**, *280*, H222–H236.
(21) Tateishi, N.; Suzuki, Y.; Cicha, I.; Maeda, N. *Am. J. Physiol. Heart Circ. Physiol.* **2001**, *281*, H448−H456.
(22) Jarvis, T. C.; Ring, D. M.; Daube, S. S.; von Hippel, P. H. *J. Biol. Chem.* **1990**, *25*, 15160–15167.
(23) Goodrich, G. P.; Helfrich, M. R.; Overberg, J. J.; Keating, C. D. *Langmuir* **2004**, *20*, 10246–10251.
(24) Sakai, H.; Hamada, K.; Takeoka, S.; Nishide, H.; Tsuchida, E. *Biotechnol. Prog.* **1996**, *12*, 119–125.
(25) Sakai, H.; Masada, Y.; Takeoka, S.; Tsuchida, E. *J. Biochem. (Tokyo)* **2002**, *131*, 611–617.
(26) Sou, K.; Naito, Y.; Endo, T.; Takeoka, S.; Tsuchida, E. *Biotechnol. Prog.* **2003**, *19*, 1547–1552.
(27) Takeoka, S.; Ohgushi, T.; Terase, K.; Ohmori, T.; Tsuchida, E. *Langmuir* **1996**, *12*, 1755–1759.